Evaluation of Perfusion Technique on Extracorporeal Circulation Based on Fluid Dynamics Using Experimental Modeling, Computational Fluid Simulation and Clinical Relevance

Ikuo FUKUDA

Medical System and Healthcare Innovation Frontier

Hirosaki University

Evaluation of Perfusion Technique on Extracorporeal Circulation Based on Fluid Dynamics Using Experimental Modeling, Computational Fluid Simulation and Clinical Relevance

Ikuo FUKUDA

A Thesis
Submitted to the Graduate School of Science and Technology In Partial Fulfillment of the Requirements for the Degree of Doctor of Philosophy in Engineering

Material Process Engineering

Graduate School of Science and Technology, Hirosaki University

(An academic adviser; Dr. Minori Shirota)

November, 2019

Contents

Chapter 1. Introduction and background

Human aorta has a three-dimensional, complex configuration with inverted U shape curve at the transverse aortic arch where arteries to head and arms originate. Flow in the aorta is pulsatile owing to cyclic ventricular ejection from the heart and aortic wall elasticity. The aorta dilates during systolic phase and contracts during diastolic phase of heart beat, known as "windkessel effect" (Segadal L. 1987). Human aorta has not a simple inverted U shape but a three-dimensional complex configuration with twisting (Morris L. 2005). Viewing from the frontal plane, the ascending aorta runs toward right-cranial direction from the heart. Then, it runs backward toward the left thoracic cavity branching three major arteries, supplying blood to the brain and upper extremities. In the left thoracic cavity, the aorta straightly goes down toward caudal direction along the vertebral column. Therefore, the ascending aorta and the descending aorta crosses in a two-dimensional projection, mimicking to cursive letter "l" (Figure 1 and 2).

Owing to this complex configuration, the aorta of aged patients frequently has cholesterol deposition on flow-separation-sites in the lumen; the lesser curvature, proximal segment of aortic arch vessels (Yamanaka K. 1995). In aged patients, aortas tend to elongate, dilate further to make more complex configuration with more significant deposits on the inner surface. In cardiovascular surgery for aged patients, prevalence of severely atherosclerotic aorta, so-called "diseased aorta", "shaggy aorta" or "hostile aorta", is increasing in proportional to patients' age (Wareing TH. 1992) (Djaiani G. 2004)(Figure 3 to 5).

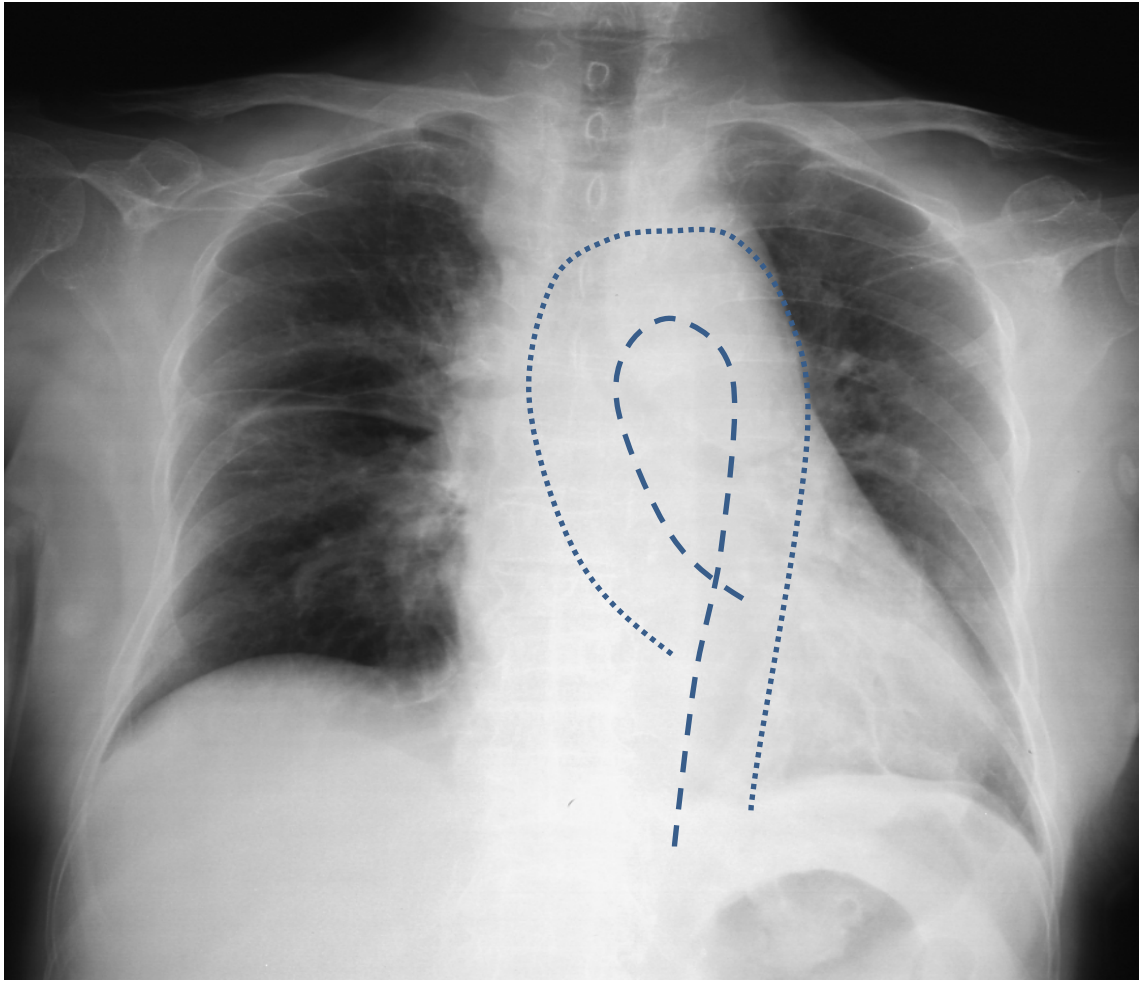Figure 1. This picture shows the chest roentgenogram on antero-posterior projection. Dotted line shows outer (small dots) and inner (large dots) outline of the thoracic aorta, with similar configuration of cursive letter "I".
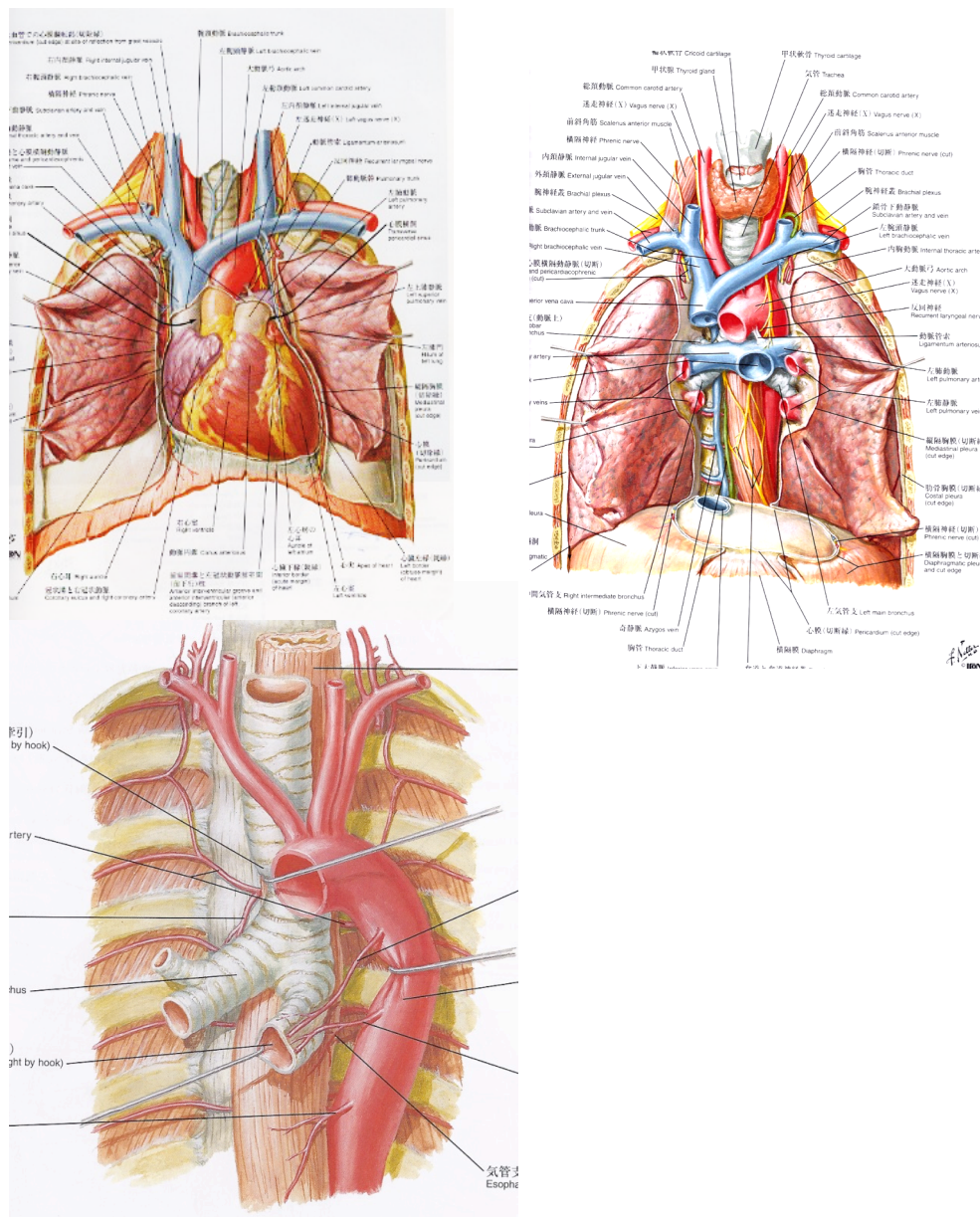
Figure 2. Anatomical view of the thoracic aorta, from the transverse aortic arch to the descending aorta, showing curved configuration of the aortic arch. (From Netter F, Atlas of human anatomy)
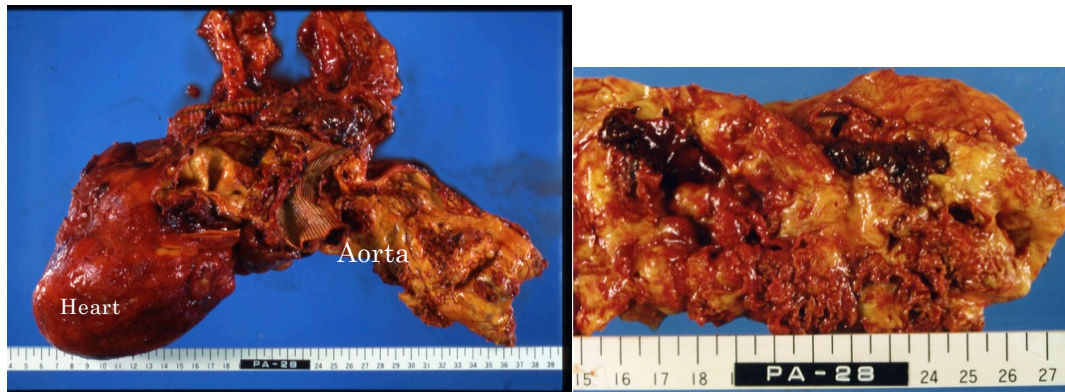
Figure 3. Left. Autopsy specimen of the ascending aorta and the transverse aortic arch in a patients with aortic arch aneurysm; Right. Magnified view of the inner aspect of the aorta, showing intimal ulcer and flail atheromatous plaque.
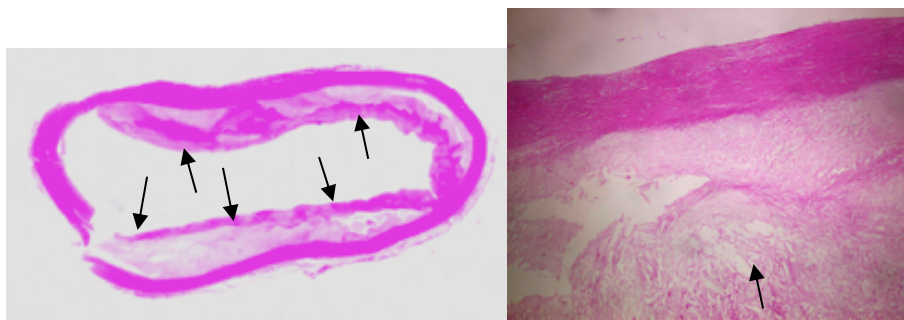
Figure 4. Left. Microscopic view of the ascending aorta in a patient with severe atherosclerosis of the ascending aorta. Black arrows indicate thickening of the media due to deposition of cholesterin crystal; Right, magnified view of the media showing degeneration of medial layer with cholesterin material which is eaten by macrophage.
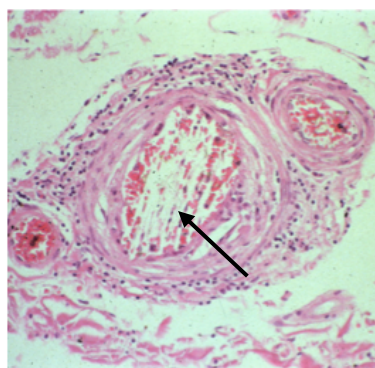
Figure 5. Microscopic view of the arteriole occluded by cholesterin emboli. Cholesterin crystal, which shows needle-like defects in the arteriole (black arrow) was washed out during staining.

10

In these two decades, outcome of open-heart surgery has drastically improved owing to progress of extracorporeal circulation technique, cardiac protection during surgery, hemostasis, development of innovative surgical devices and improvement of perioperative management, even though candidates for cardiovascular operation has been getting older. However, aged patients tend to have atherosclerotic degeneration of great vessels, especially on the aortic arch and the descending aorta. In surgery for atherosclerotic cardiovascular disease such as ischemic heart disease or thoracic aortic aneurysm, extracorporeal circulation is essential technique for repair of intracardiac or aortic lesions. Extracorporeal circulation requires drainage of venous blood from two great veins draining into the heart; the superior vena cava and the inferior vena cava. Venous blood, which has low oxygen content, goes out from these venous drainage tubes by gravity during heart surgery. Then oxygenation and decarbonation is accomplished by artificial lung by diffusion of gases through the thin silicon membrane. The oxygenated blood is returned into the arterial system through the ascending aorta or peripheral arteries such as the femoral artery, via arterial perfusion cannula. Diameter of the arterial perfusion cannula is as small as 7 or 8mm, one thirds of the normal aortic valve diameter, which is larger than 20mm in normal adult; the cross-sectional area of the left ventricular outlet is larger than 3 cm². Therefore, flow velocity from small diameter perfusion cannula is fast. Energy of this jet flow is larger than that in normal aorta. In case of healthy aorta with smooth and elastic inner surface, this jet flow does not injure the inner surface of the aorta, called the "intima". However, in case of the aged patients, the intima of the aorta tends to have degenerative change by atherosclerosis. A jet from a small caliber aortic perfusion cannula may collide with aortic wall, causing detachment of frail plaque and resulting in atheroembolism to systemic organs (Katz ES. 1992)(Fukuda I. 2007). Embolic stroke caused by "sandblast effect from the cannula jet" is an emerging problem in cardiovascular surgery using cardiopulmonary bypass (Ura M. 2000). Stroke occurred in 2.3% to 6.0% of patients who underwent cardiovascular surgery using extracorporeal circulation (Hosoda Y. 1991) (Almassi GH. 1999) (Groom RC. 1995). According to research on risk factor for stroke in

cardiac surgery, prolonged cardiopulmonary time was a significant perioperative predictor of stroke (McKhann GM. 1997), (Almassi GH. Ann Thorac Surg 1999). Blauth et al. reported severity of atheroma in the ascending aorta and the aortic arch was significantly related with postoperative stroke (Blauth CI. 1992). In the analysis of 211 autopsy patients who had undergone coronary artery bypass or valve operation, atheroemboli were identified in 48 patients (21.7%), and multiple atheroembolism was noted in 30 (62.5%) out of these 48 patients. The atheroembolic stroke was found in 21 (16.3%) of 129 patients whom the autopsies including the brain were completed. Atheroembolic events were highly correlated with the atherosclerosis of the ascending aorta; atheroembolic events occurred in 46 of 123 patients (37.4%) with severe disease of the ascending aorta while it occurred only in 2 of 98 patients (2%) without significant ascending aortic disease. According to the evaluation of the ascending aorta in 1,735 patients, atherosclerosis was found in 152 patients (8.8%) with mild (4.5%), moderate (2.2%) and severe (2.0%) grade (Mills NL. 1991.). Therefore, pre- or intra-operative evaluation of the ascending aorta was essential to prevent stroke due to atheroemboli detached from the aortic wall, particularly in the operation using ECC. However, we have not known about hydrodynamics during ECC even though it had good correlation with atheroembolic events.

Many investigators have studied about the visualization of flow pattern in the aorta using several kinds of techniques and materials. Endo et al. had perfused a transparent aortic model under a steady flow, and visualized the intra-aortic flow by analyzing the movement of tracers by cinemicrography (Endo S. 1996). Yearwood and colleagues had investigated the flow patterns in a human aortic arch model during pulsatile flow (Yeawood TL. 1984). Recent advance in magnetic resonance imaging has demonstrated three-dimensional mapping of velocity and flow pattern of in-vivo intra-aortic flow throughout systolic and diastolic phase (Kilner PJ. 1993). It revealed that physiological flow in the aorta was characterized by helical and retrograde flow. Other investigators have been trying to simulate blood flow in the aorta computationally, and reproduced physiological flow pattern in the aorta (Mori

D. 2002) (Shahcheraghi N. 2002) (Chandran KB. 1993).

The aim of our studies is to clarify shear stress distribution in the aortic arch and to elucidate mechanism of atheroembolism due to sandblast effect of the jet flow using the glass aortic model and computed simulation model. In Chapter 2, we will show results of experimental studies using glass aortic arch models and particle image velocimetry (PIV). In Chapter 3, we will show in vivo study of flow velocimetry using intraoperative duplex echography. In Chapter 4, we will show results of computed flow simulation. In Chapter 5, we will discuss future of flowdynamic study and application of flowdynamics in cardiac surgery.

Chapter 2. Flowdynamics of arterial perfusion in a glass aortic model

Section 1. Aortic perfusion in the normal aorta

1. Materials and Methods

1) Flow velocimetry in glass aortic model

i. Creation of an aortic model for particle image velocimetry method

Initially, we tried to use an aortic arch model made by polyvinyl chloride which was sold in the market for medical education. The advantage in using this model was high-transparency and elasticity of the wall material. However, tracer particles have stuck to the wall of the aortic model during preliminary perfusion experiment; therefore, we abandoned our attempt to use this model. Then, we made an epoxy-resin model of the human aorta using a laser modeling method, three-dimensional CAD software (Mimics, Materialise, Yokohama, Japan) and a laser modeling system (SCS-8100/8100D, D-Mec Ltd., Tokyo, Japan). These models reflected real shape of the human aorta; however, transparency of the epoxy-resin was very low due to irregular surface of the model (Figure 6A). It was also not water proof. As the result, these models were not appropriate as modelling for PIV method. Finally, we made glass aortic arch models to mimic aortic models made from thin-sliced CT images of a healthy adult and of a patient having transverse aortic arch aneurysm (AAA) (Figure 6B). In the series of our experiments, we used this glass aortic model.
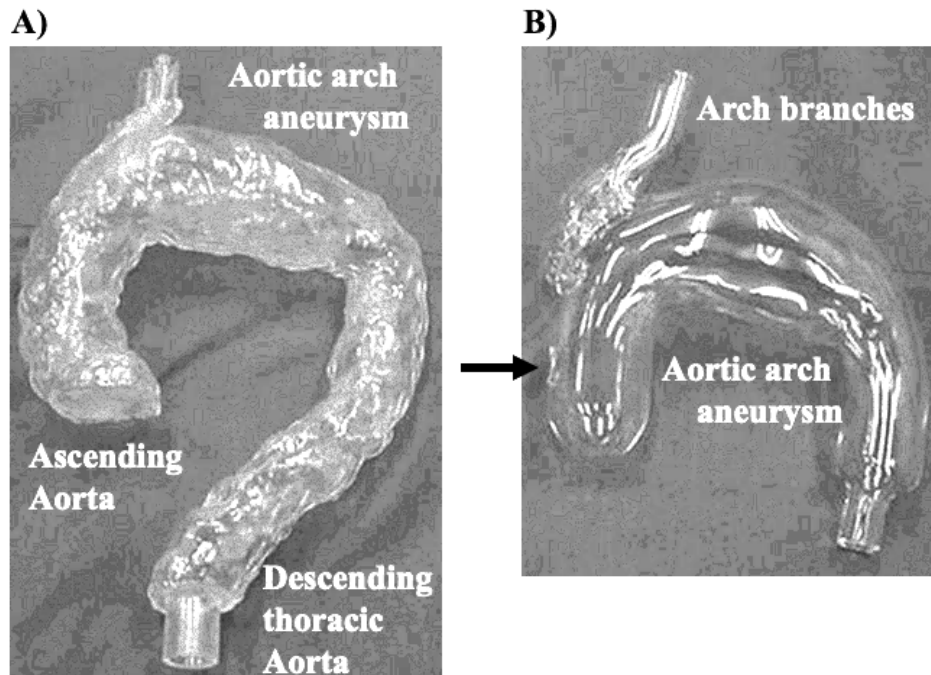
Figure 6. Left, Three D model of an aortic arch aneurysm using 3D printing; Right, glass aortic model for PIV measurement.

In normal aortic model, the outer diameter of the aorta and the three aortic arch branches were 30 and 8.5 mm, respectively. Aortic cannulation site of 8.5 mm in diameter was created at the outer wall of the ascending aorta 4 cm proximal to the origin of the brachiocephalic artery (BCA). We divided the aortic arch into three segments to establish the following morphological regions: before the orifice of the BCA; proximal arch, between the orifice of the BCA and the left subclavian artery (LSCA); middle arch, distal segment from the orifice of the LSCA; distal arch. The aortic arch model was made from enhanced CT of a 73-year-old patient with an atherosclerotic transverse aortic arch aneurysm.

The following circuit was prepared for ECC. Water, in temperature ranging from 21.4 to 23.0°C, was perfused into the aortic model by a centrifugal pump (HPM-15, Nikkiso, Co., Ltd., Tokyo, Japan) powered by a Nikkiso motor (HAP-21, Nikkiso, Co., Ltd.), into the ascending aorta via the cannula. Simulated extracorporeal circulation system was established using centrifugal pump (Figure 7). The model was placed

15

into a transparent glass tank filled with water. The perfusate from the three arch branches and the descending aorta were drained into a water chamber. Non-pulsatile arterial perfusion was performed thorough 7mm cannula in the ascending aorta. Flow velocity, shear stress and flow vector were measured using particle image velocimetry (PIV method). Perfusion rate was set at 4.0 L/min of steady flow and the perfusion pressure was maintained from 60 to 80 mmHg by compressing the circuit tube that collected effluent from the three arch branches, using pincher to control the circuit resistance. The circulation pressure was monitored by a pressure monitor connected to a circuit tube from the arch branches. The water from the three branches was drained into the same reservoir. Approximately 15 to 20% of total flow went into arch vessels under this condition.

Figure 7. Glass aortic models (left upper plate; normal aortic model, left lower plate; aortic arch aneurysm model) and perfusion circuit. Aortic cannula and flowmetry in mock circulation system

ii. Particle image velocimetry (PIV)

The PIV system consisted of the following four elements: double pulse Nd:YAG laser emitter (Solo II-15, New Wave Research, Inc., CA, USA), cross correlation camera (MEGAPLUS model ES1.0, REDLAKE MASD, Inc., CA, USA), laser pulse synchronizer (Laser Pulse, TSI, Inc., Minn, USA) and PIV analysis software (INSIGHT version 3.34, TSI, Inc., Minn, USA). High porous polymer (MCI GEL HP20P, Mitsubishi chemical, Co., Tokyo, Japan) of 75 to 150 micrometers in diameter were mixed in water as the tracer. Sheet-like-formed double-pulsed laser (wavelength, 250nm; laser light frequency, 15Hz; double pulse interval, 500 microsecond (μ sec); power, 500W) was emitted to the aortic arch model that was set

in water tank in order to visualize the perfusing tracers reflected by laser beam. Then, the image of the tracers was captured by cross correlation CCD camera that was synchronized with the double-pulsed laser emission by a synchronizer. The movement of tracers in 500 micro-sec was expressed as the vectors of 2 directions (x- and y-axis) by PIV analysis software.

The measurement was performed in the longitudinal and horizontal section of the aortic model. The longitudinal image was captured on the condition that the sheet-formed laser beam passed the midline of both the ascending and descending thoracic aorta including the orifices of the three aortic arch branches. The horizontal image was captured in every 5 mm from the cannulation site along the outer curvature of the aortic arch.

iii. Flow image and velocity mapping

a) Flow image, velocity mapping and Urms value

The velocity mapping and flow image by streamlines were constructed from mean velocity (U) and directions of vectors of 30 to 80 consecutive images, as defined by the following equation.

$$U = \frac{1}{n}\sum_{i=1}^{n} u_i$$

The velocity mapping was expressed by color gradients from blue to red, ranging from 0 to over 1m/sec, respectively.

Using this mean velocity (U), variance (VA) was calculated by the following equation.

$$VA = \frac{1}{n}\sum_{i=1}^{n} u_i^2 - nU^2$$

Then, the rms value (m/sec) that means velocity fluctuation or degree of velocity turbulence was expressed by the following equation.

$$Urms = \sqrt{VA}$$

Streamline and flow velocity was depicted in the longitudinal plane and short

17

axial plane perpendicular to longitudinal axis. Distribution of flow velocity was depicted in color mapping in two directions expressed by color gradients from blue to red ranging from 0 to over 1m/sec, respectively. Short axial view could not be obtained within 20 mm from cannula tip due to the shadow of the descending aorta and cannula. Short axial flow pattern was taken in 7 points as shown in the figures 3-6.

b) Magnitude of strain rate tensor

Magnitude of strain rate tensor was calculated using the data of distance vector (X, Y) and velocity vector (U, V) and those were calculated by PIV analysis software. Strain rate tensor is expressed as the following equation:

$$D_{ij} = \frac{1}{2}\left(\frac{\partial U_i}{\partial X_j} + \frac{\partial U_j}{\partial X_i}\right)$$,

and components where i and j are changed from 1 to 2 are expressed as follows:

$$D_{11} = \frac{1}{2}\left(\frac{\partial U}{\partial X} + \frac{\partial U}{\partial X}\right) = \frac{\partial U}{\partial X}$$

$$D_{12} = \frac{1}{2}\left(\frac{\partial U}{\partial Y} + \frac{\partial V}{\partial X}\right) = D_{21}$$

$$D_{22} = \frac{1}{2}\left(\frac{\partial V}{\partial Y} + \frac{\partial V}{\partial Y}\right) = \frac{\partial V}{\partial Y}$$,

then the magnitude of strain rate tensor is calculated by adding those components as following.

$$|D| = \sqrt{2D_{11}^2 + 2D_{12}^2 + 2D_{21}^2 + 2D_{22}^2}$$

The measurement was performed in the longitudinal and horizontal section of the aortic model. The longitudinal image was captured on the condition that the sheet-formed laser light passed the midline of both the ascending and descending thoracic aorta including the orifices of the three aortic arch branches. The horizontal image was captured every 5 mm from the cannulation site along the outer curvature of the aortic arch.

d. Aortic perfusion cannula

Five types of aortic perfusion cannula were tested. As non-dispersive type, curved end-hole cannula with 45-degree angle (TOYOBO OUKN-L-7.3mm, TOYOBO, CO., LTD., Osaka, Japan) was tested. As the first-generation dispersive cannula, Dispersion cannula® DCT21A (Edwards LiveScience LLC, Irvine, CA, USA) and Sarns Soft-Flow model 5767, 7.0mm (3M Cardiovascular, Ann Arbor, MT, USA) were tested. While the former cannula generates fan-shaped attenuated flow, the latter generates multiple jet-streams. As the second-generation dispersive aortic perfusion cannula, EZ glide (Edwards LS) and Stealth-flow ™ (Toyobo) cannula were tested (Fig 8). These cannulas generate three-dimensional, flame-shape attenuated flow from the cannula tip. Distribution of flow velocity, shear stress and degree of turbulence were evaluated using PIV method. Flow patterns, shear stress and velocity at the ostium of arch vessels was measured and compared in each cannula.
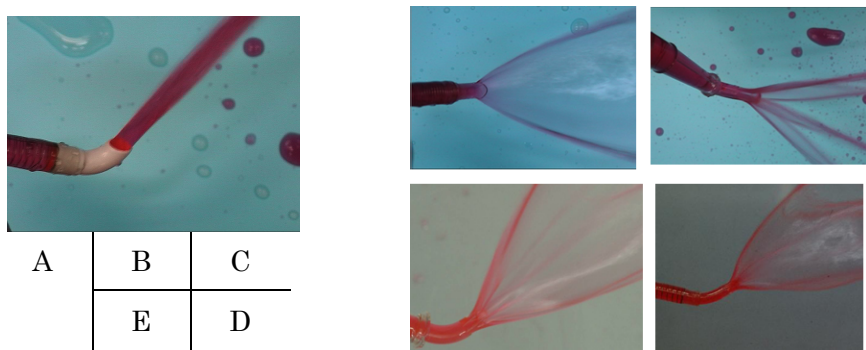

Figure 8. Aortic perfusion cannula. A, End-hole cannula; B, Dispersion cannula; C, Soft-Flow cannula;D, Stealth-flow cannula; E, EZ glide

Results

In end-hole cannula, swift flow with maximum velocity of 70cm/sec rushed linearly without deceleration, and collided with outer curvature of the distal aortic arch (Fig 9). After hitting the aortic wall, decelerated flow made reversed vortical flow going toward the distal arch and inner curvature. Some stream regurgitated to the proximal arch and went into the left carotid artery. Steady flow was observed in the descending aorta. Turbulent flow and strong shear stress were observed on the outer curvature of the aortic arch.

In first generation dispersive type cannula, heterogeneous flow was generated from cannula tip. Although small peak of flow velocity and shear stress was observed on the lesser curvature, flow velocity was generally slower than that in end-hole cannula (Table 1). In 2nd generation dispersive cannula, flow velocity was very slow around brachiocephalic artery ostium and left common carotid artery ostium.

As a representative of dispersive cannula, flow map, degree of turbulence and shear stress distribution of Dispersion cannula was shown in Figure 10. Flow from cannula tip generated thin membranous jet. Although flow velocity at the exit of the cannula was fast, it decelerated within several cm from the exit. High shear stress peak was observed at lesser curvature of the transverse aortic arch.
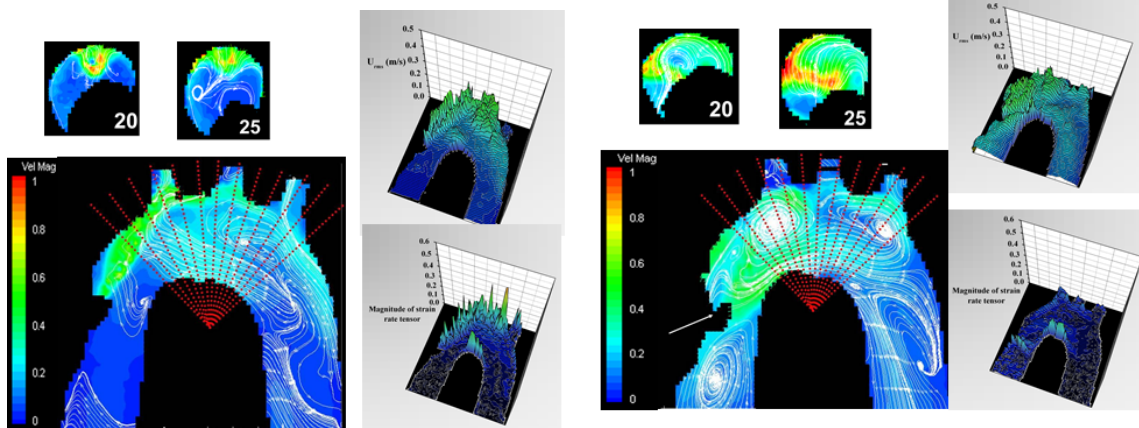
Figure 9. Flow velocity map (left plates), degree of turbulence (right upper plate) and distribution of shear stress (right lower plate) of flow from end-hole cannula.

Figure 10. Flow velocity map (left plates), degree of turbulence (right upper plate) and distribution of shear stress (right lower plate) of flow from Dispersion cannula.

	Classic	1st generation		2nd generation	
Flow velocity (m/s)	EH	DSP	SFT	EZG	STL
Brachiocephalic artery	0.7	0.5	0.3	0.3	0.2
Left common carotid artery	0.5	0.3	0.2	<0.1	0.1

Table 1. Maximum flow velocity at the ostium of major arch vessels in each cannula. EH; end-hole cannula, DSP; Dispersion cannula, SFT; Soft-Flow cannula, EZG; EZ glide cannula, STL; Stealth-flow cannula

Discussion

Tested aortic cannulas in this study are characterized by specific exit shape which brings about different stream dynamics. Curved end-hole cannula brings about simple straight jet stream. Dispersion cannula, Soft-Flow cannula and SELECT 3D cannula are designed to reduce flow velocity by forming a dispersed jet stream. Several studies have investigated the correlation between end-hole cannulas and stroke. Weinstein and colleagues reported that perioperative stroke occurred in 24 of 2217 patients, and the stroke area in brain appeared more in the left hemisphere (75%) than in the right (25%) (Weinstein GS. 2001). They indicated that a disproportionate occurrence of stroke area would be the result of a high-velocity jet from end-hole cannula directing at the orifice of the left common carotid artery. They had not experienced stroke since they had begun to use the dispersive type cannula. In the study that compared prevalence of stroke in straight and bent-tip end-hole aortic cannula cases, the incidence of stroke was significantly higher in end-hole cannula (1.8%) than in bent-tip cannula (0.9%) (Albert AA. 2002). The severity of stroke was related to the use of straight cannula, because the high-velocity jet blew directly at the posterior wall of the ascending aorta. The dissected atheroemboli would go up into the brain through the aortic arch. The prevalence of bilateral and posterior strokes was significantly high with the use of straight cannulas, while there was no bilateral or posterior stroke in the bent-tip cannula cases because the jet becomes attenuated before the orifices of aortic arch branches.

There are many cannulas with multiple jet-streaming or dispersing types designed for reducing exit force against the aortic wall, and there are many reports investigating the characteristics the cannula. Groom and colleagues measured the peak flow of cannular jet under the condition of steady and pulsatile flow in the silicon aortic model using a laser Doppler velocimetry system (Groom RC. 1995). The exit velocity of the Soft-Flow cannula was the slowest both in steady and pulsatile flow among five cannulas. Muehrcke and colleagues tested six types of cannulas in a closed circuit perfused with centrifugal pump, and revealed that peak velocity (288 ± 51cm/sec) and exit force (0.12 ± 0.44Newtons) of the Soft-Flow cannula was

significantly less than other cannulas with no increase in the hemolysis (Muehrcke DD. 1995). Furthermore, in vivo intraoperative analysis by transesophageal echocardiography demonstrated the superiorities of the Dispersion cannula by reduction of flow velocity among three types of aortic cannulas; end-hole cannula, Soft-Flow cannula and Dispersion cannula. They noted that it significantly reduced exit velocity (Grooters RK. 2003).

In the curved end-hole cannula, we found high-velocity jet reaching to the orifices of the arch branches without attenuating its velocity as previous reports (Weinstein GS. 2001), (Albert AA. 2002). This high-velocity stream appeared not only along the large curvature of the aortic arch but also in the arch branches. In these regions, the shear stress was also high. In the straight end-hole cannula, high-velocity jet was directly blowing against the posterior wall of the ascending aorta, and a large clockwise helical flow was observed from the ascending aorta toward the aortic arch with an increased shear stress near the ascending aortic wall. Moreover, shear stress was high near the posterior wall of the aortic root where a downward stream was created. These characteristics of end-hole cannula coincide with the increased possibility of perioperative embolic strokes. Huebner and colleagues investigated the arch vessel pressure and flow distribution comparing a curved end-hole cannula, Soft-Flow cannula and Dispersion cannula in the glass aortic arch model (Joubert-Huebner E. 2000), (Joubert-Hubner E. 1999). When the cannular jet stream was directed toward the BCA, flow and pressure in the BCA was higher than the initially set values, while flow and pressure in the other arch branches were similar or smaller. This imbalance in flow and pressure was the largest in the end-hole cannula. In the present study, the jet stream from the end-hole cannula went toward the BCA; however, there was a downward streamline along the inner wall of the LSCA.

The characteristic of the Dispersion cannula is the fan-shaped exit flow. In this study, exit flow was attenuated at 3 cm from the cannular tip before the orifice of the BCA, but the laterally spreading jet reached to the arch wall where high shear stress was created along the ascending aortic wall. In addition, around the secondary large vortices near the orifice of the BCA and the LSCA, increased shear stress area

was found. Flow imbalance in the LSCA was also found as downward stream along the outer wall in the LSCA.

The exit flow of the SELECT 3D cannula was characterized by a complex of flows from three skewed-opening side-holes and one end-hole, which resulted in a complex flow velocity of lesser intensity from the side of the cannula while the central exit velocity remained high. Besides the variation in flow velocity, the cannular tip is bent at 45 degree to prevent the exit flow from blowing directly at the posterior wall of the ascending aorta. An important point about this cannula was that neither increased velocity nor shear stress was found near the arch branches. However, there was a possibility for injuring atheromatous plaque on the inner curvature of the aortic arch, where increased shear stress was found.

The Soft-Flow cannula is characterized by laterally blowing jets from four skewed-opening side-holes contributing to reducing "sandblasting" effect of blood exiting the aortic cannula, and resulting in lower exit force and flow velocity. In this study, the attenuation of exit flow velocity was the most marked among the other cannulas, and the shear stress along the large curvature of the aortic arch was not increased. These characteristics are beneficial to reduce atheroembolic events. The potential concern of Soft-Flow cannula was that one of the exit flows reached to the posterior wall of the ascending aorta without attenuating its high velocity, so disruption of atheromatous plaque may occur.

Limitation of this study

There is a concern about perfusate that may affect flow analysis in this model. We used water as perfusate that has viscosity much less than blood; therefore, the Reynolds number that influences the flow pattern in the "steady flow" becomes lower than in in-vivo. However, the Reynolds number of jets at cannular exit was about 14,400 that was recognized as "turbulence flow", so it was considered that the analysis of flow pattern would be almost the same as that of in-vivo conditions because the turbulence flow never changes into a steady flow.

Conclusion

In conclusion, the multiple-jet streaming cannula or dispersion cannula is less invasive on the aortic wall than the end-hole cannulas, and thereby could potentially contribute to a decreased risk of perioperative stroke. We should choose a cannula based upon flow patterns of cannulas. We should also pay special attention to selection of cannulation site according to the atherosclerotic pattern of the ascending aorta and the aortic arch.

Section 2. Flowdynamics of aortic perfusion in a AAA model

In the previous section, we investigated intra-aortic flow dynamics during ECC, using a glass thoracic aortic model by means of PIV method. We elucidated particular flow dynamics during ECC, with five different types of aortic cannulas in a normal aortic model. We demonstrated the flow from dispersive type aortic cannula is the softest against the aortic wall by sudden attenuation of the flow velocity and stress. However, analysis of flow dynamics in an aortic arch aneurysm (AAA) has never been performed.

In this section we investigated flow pattern, velocity and tensor of strain, a function of shear stress, in a AAA model. Using a AAA model, we analyzed the effect of cannula-tip-shape on the flow in the thoracic aorta, especially on the aneurismal wall and ostium of the aortic arch vessels. The aim of this study is to establish a new method for evaluation of arterial cannulas, and to elucidate a safe perfusion method in the diseased aortic arch.

Materials and Methods

The glass AAA model duplicated the three- dimensional contour of the aortic arch having AAA was made (see, Section2, Fig 7). The inner diameter of the ascending aorta and the three aortic arch branches were 35 and 8.5 mm, respectively. A cannulation site of 10 mm in diameter was created at the outer wall of the ascending aorta 4 cm proximal to the origin of the brachiocephalic artery. Although the maximal outer diameter of the AAA was 6cm, the major part of the AAA was obliterated by mural thrombus. Therefore, the diameter of the AAA glass model at the aneurysmal site showed the inner surface of aneurysm, around 4.5cm (Fig 11).
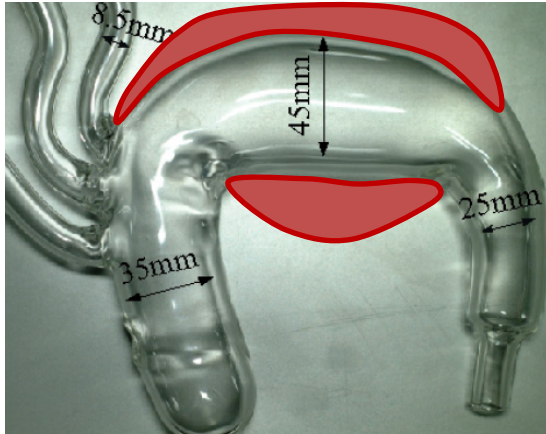
Fig 11. Glass AAA model. The model reproduces only inner lumen of the aneurysm. There is thick "mural thrombus" on dilated portion of the transverse aortic arch (red area).

The setting of ECC perfusion was same as described in Chapter 2, Section 1. We tested the following three aortic cannulas: a curved end-hole type cannula with a 45° angle (Toyobo OUKN-L-7.3 mm, Toyobo, Co., Ltd., Osaka, Japan); a Dispersion cannula (RMI DCT21A-21 Fr, Research Medical, Inc., Midvale, UT, USA) and a Sarns Soft- Flow model 5767-7.0 mm (3M Cardiovascular, Ann Arbor, MI, USA) as the multiple jet-stream cannula (Fig 12).
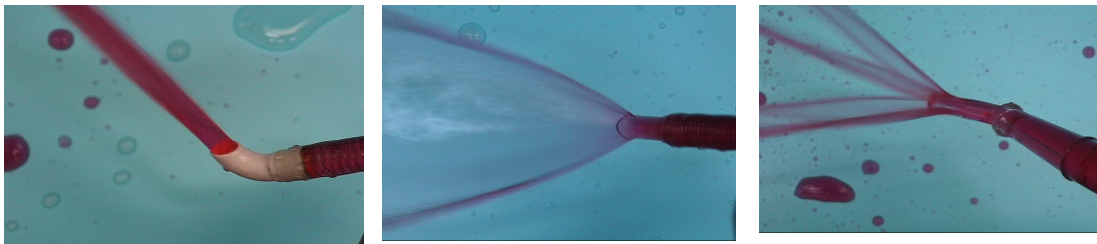
Fig 12. End-hole cannula, Dispersion cannula and Soft-flow cannula.

Visualization of flow pattern

Visualization of perfusate in the aortic arch model was performed by a PIV method as shown in previous section. The model was set in a water tank in order to visualize the perfusing tracers by the laser.

The measurement was performed in both longitudinal and horizontal sections of the AAA model. The longitudinal image was captured on the condition that the plane

of laser light passed through the midline of both the ascending and descending thoracic aorta, including the orifices of the three aortic arch branches. The horizontal image was captured every 5 mm from the cannulation site along the outer curvature of the aortic arch.

Results

In the longitudinal axis, vortices of varying sizes were appeared during simulated ECC. Secondary flow was observed in the short axial view. Of note, streamline, secondary vortices, and helical flow patterns were not similar between the three cannulas.

Curved end-hole cannula

In the curved end-hole type cannula, the cannular jet streamed at a steady velocity ranging from 0.6 to 0.8 m/s towards the aneurismal wall, where thick mural thrombi existed. Large vortices were created on the proximal and distal site of the main stream. Flow decelerated and reversed near the aortic arch branches. A steady flow pattern was observed in the descending aorta. Velocity fluctuation (Urms) was increased as well as the strain rate tensor ($|D|$ = ~0.2– 0.25/s) (shear stress) in the outer curvature of the aortic arch aneurysm (Fig.13).
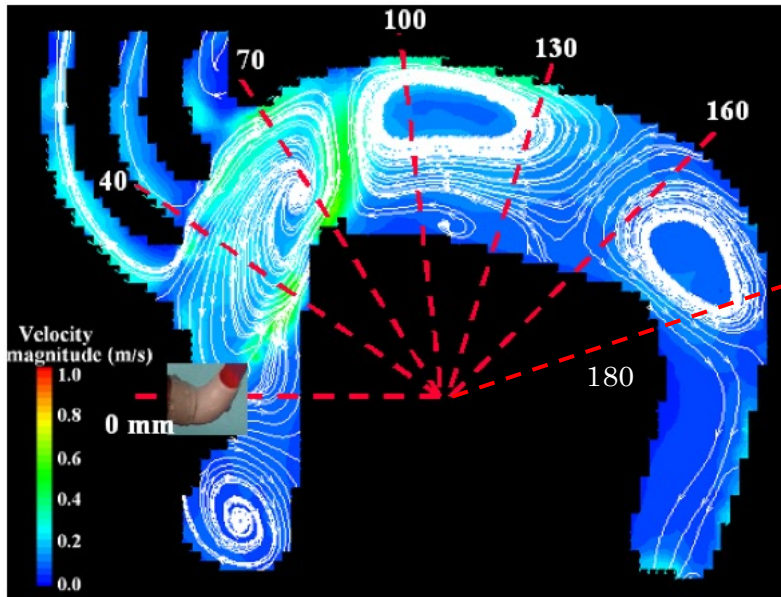
Fig 13. Measurement points of a AAA model. The transactional planes at each point from the aortic cannula was shown around the longitudinal plane.
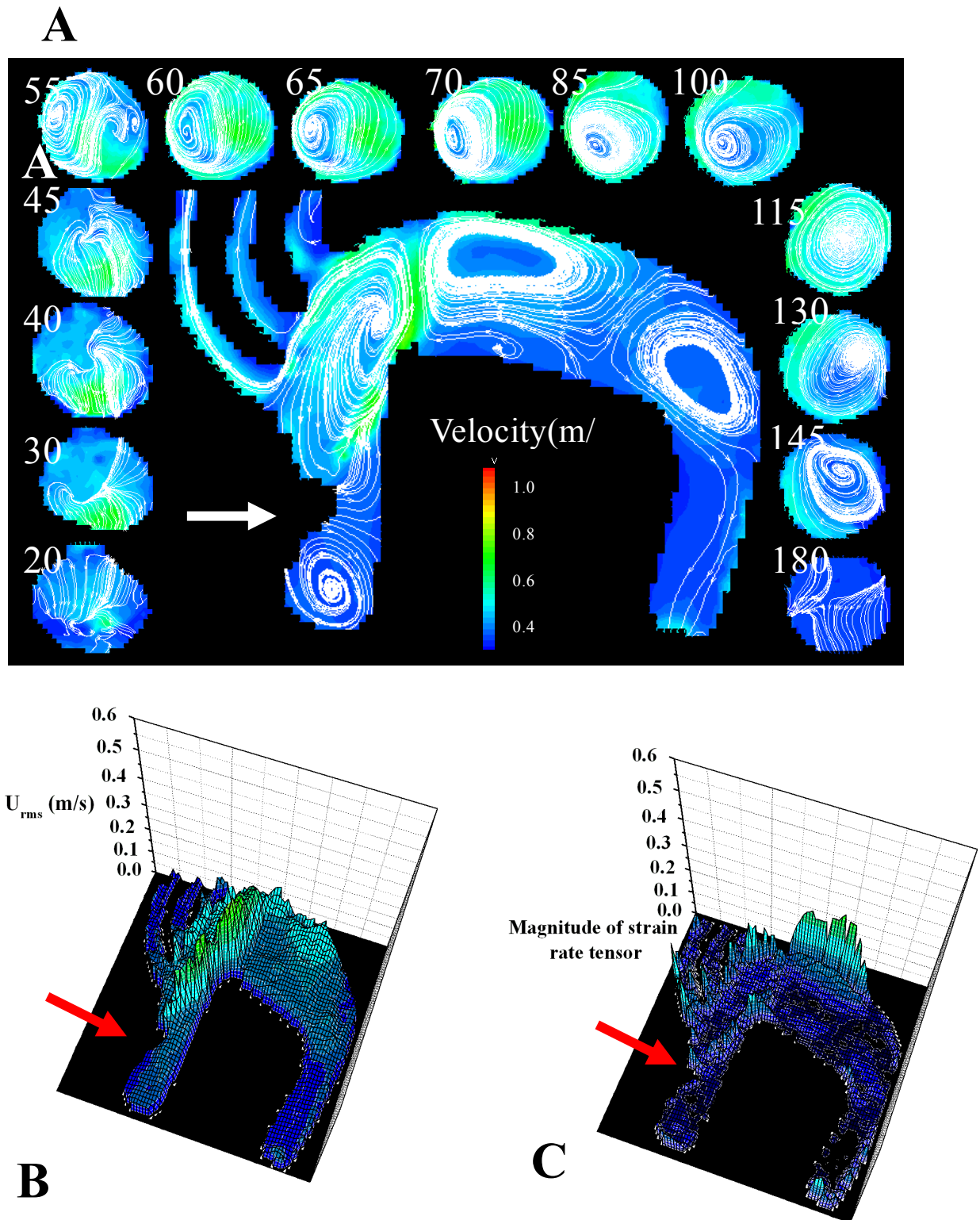
Fig 14. A, streamline of a flow from the endohole cannula; B, degree of turbulence;
C, magnitude of strain tensor in the longitudinal plane

Dispersion cannula

In Dispersion cannula, a fan-shaped swift flow pattern was observed in the center of the ascending aorta, with a velocity less than 0.5 m/s (Fig.15A). Swift stream was attenuated within the aneurysm. Large vortices at slow velocity were observed in both the aneurysm and descending thoracic aorta. Reversed vortical flow in the ascending aorta streamed into the arch vessels. Although turbulent flow with increased velocity fluctuation (Urms) (less than 0.1m/s) was observed in the ascending aorta, a strain rate tensor (|D|) (shear stress) in the aneurysm was small (less than 0.15/s) (Fig.15B,C).
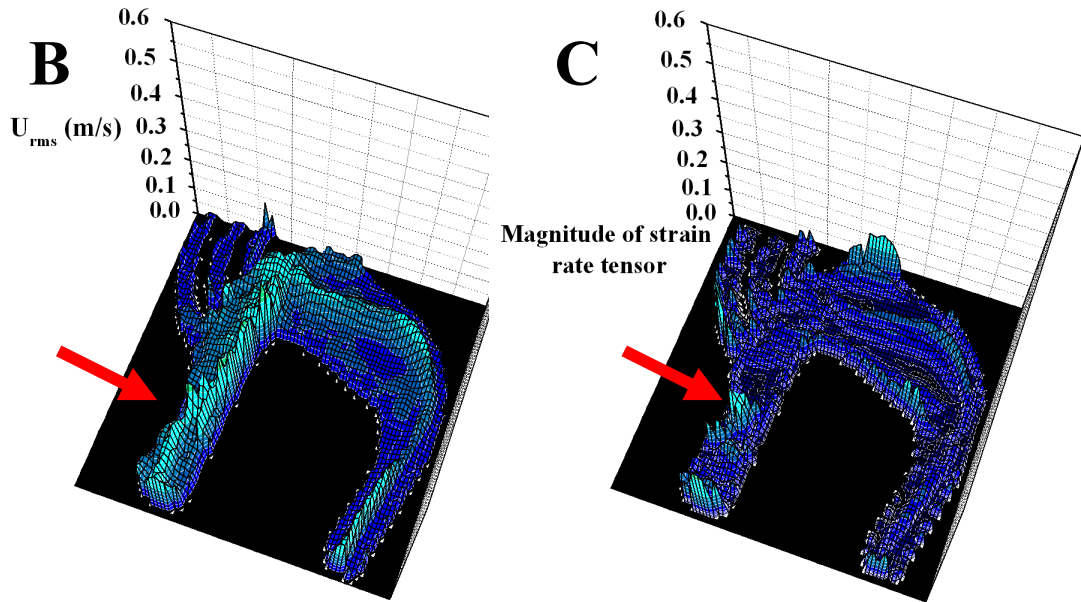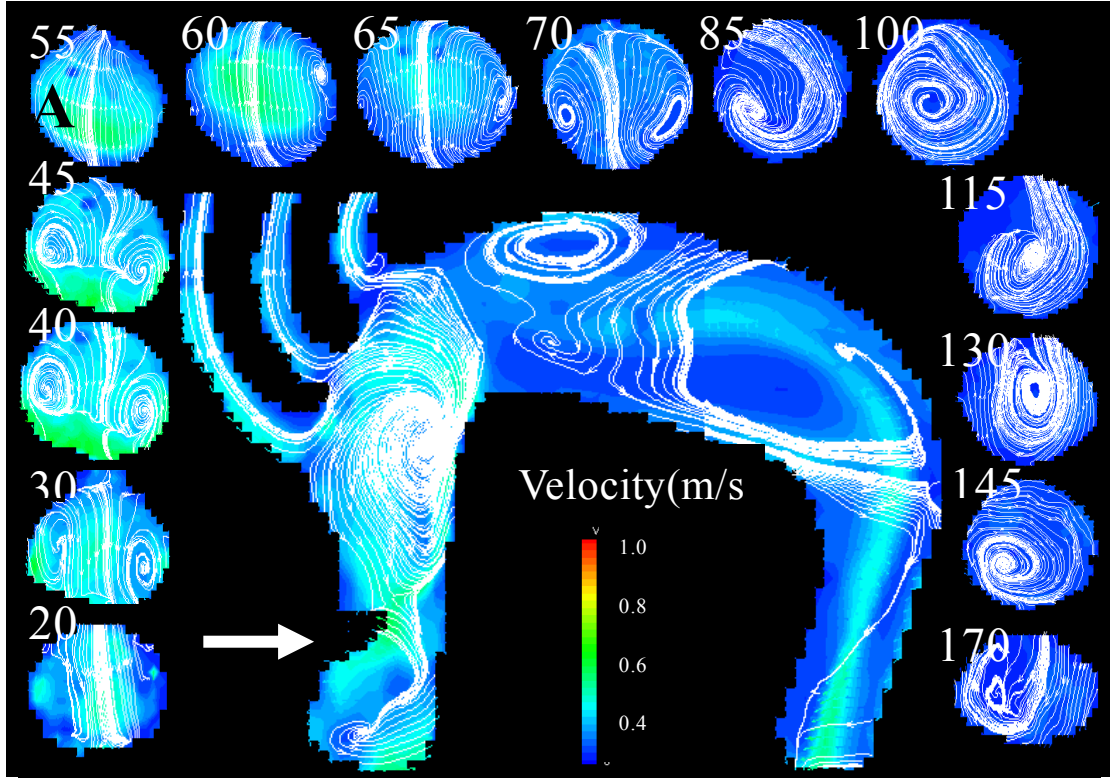
Fig 15. A, streamline of a flow from the Dispersion cannula; B, degree of turbulence; C, magnitude of strain tensor in the longitudinal plane

Soft-Flow cannula

In the Soft-Flow cannula, multiple jets, each with a velocity less than 0.5 m/s were observed at the cannula outlet (Fig. 16A). Similar to the Dispersion cannula, swift stream was attenuated in the ascending aorta, and large vortices with small velocities were observed in both the aneurysm and descending thoracic aorta. Likewise noted was a reversed vortical flow in the aortic arch with runoff into the arch vessels. Velocity fluctuation (Urms) was unchanged at 0.2 m/s and a small (less than 0.15/s) strain rate tensor (|D|) (shear stress) was noted in the aneurysm (Fig. 16B, C).
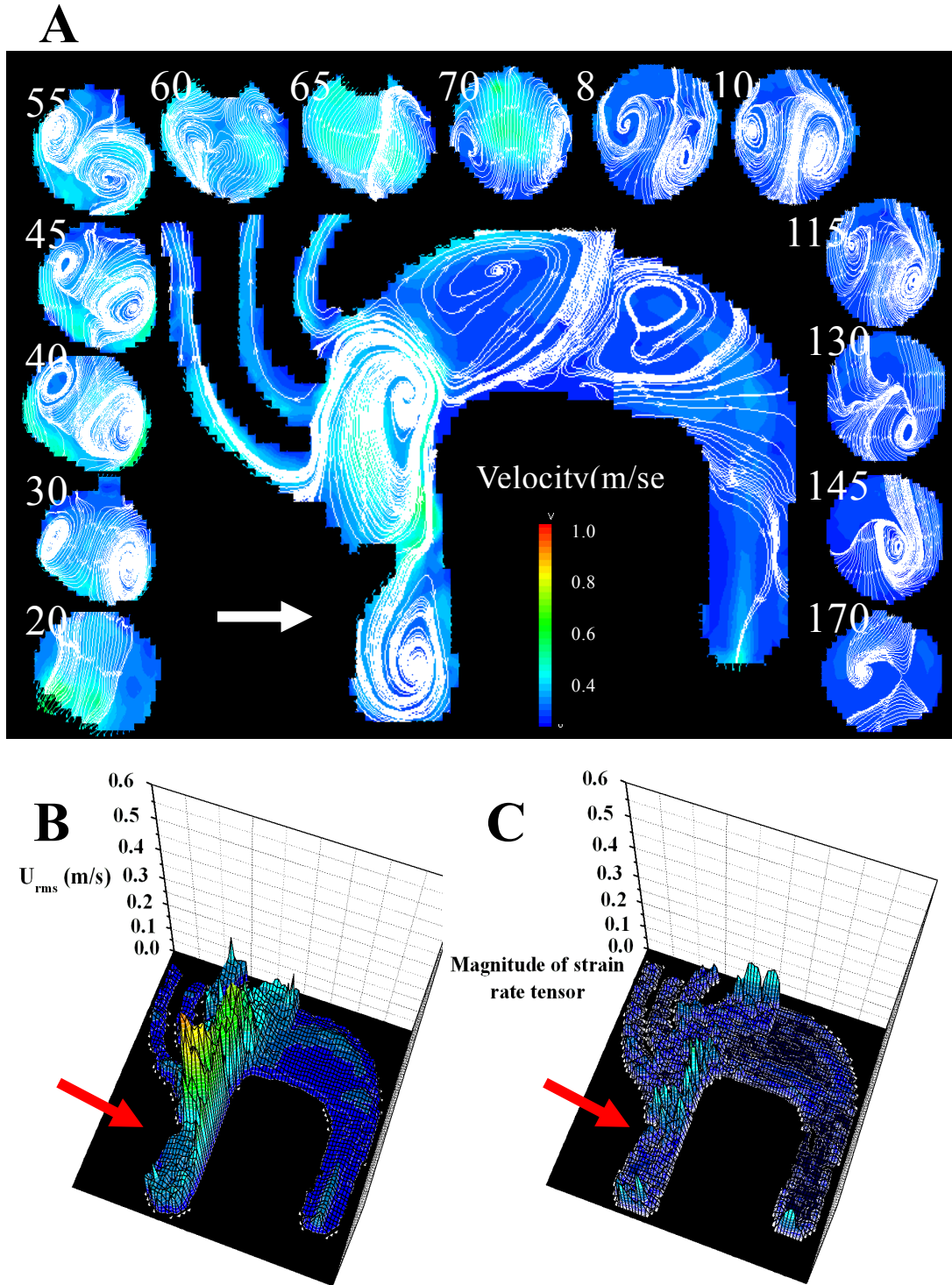
Fig 16. A, streamline of a flow from the Softflow cannula; B, degree of turbulence; C, magnitude of strain tensor in the longitudinal plane

Discussion

The preceding study showed our understanding of intra-aortic flow characteristics with different cannular structures, cannular jet exit forces on the aortic wall of a aortic arch model. This experiment on AAA model showed differences of flowdynamics between normal aortic arch model and a AAA model.

In cases of total arch replacement, the incidence of permanent neurological deficits is 0.8 to 8.7% (Numata S. 2003) (Kazui T. 2007)(Ueda T. 2003) (Okita Y. 2001). Significant perioperative risk factors for stroke in cardiac surgery include the use of cardiopulmonary bypass or a prolonged cardiopulmonary bypass time (Almassi GH. 1999) (McKhann GM. 1997) (Sharony R. 2004). Atheroma load in the ascending aorta and aortic arch was also significantly related to stroke rates (Hosoda Y. 1991) (Blauth CI. 1992). Existing data suggest that manipulation-related stroke occurred in the right side of the brain after cardiac surgery with ECC; however, cannulation-related atheroembolic stroke occurred in the left side of the brain, where accelerated jet flow hit around the ostium (Ura M. 2000). Strain rate tensors were relatively high, even with the dispersion-type aortic cannula, especially in the posterior wall of the ascending aorta, where the atherosclerotic load tends to be higher.

Our study provided a better understanding of aortic perfusion. First, cannular jets from a curved end-hole cannula are blown towards the distal arch and hit the outer curvature of the aortic arch where thick mural thrombi and fragile atherosclerotic lesions frequently exists. Arch vessels are often displaced towards the ventral side due to elongation of the transverse aortic arch. The cannula jet blows along the inner curvature of the aortic arch towards the distal aortic portion. Furthermore, cannular jets blow by skimming the inner curvature, where the atherosclerotic load is often severe due to flow stasis, in patients with arch aneurysms. Akin to the conclusion from a previous study, use of dispersion-type cannulas should be cautious in atherosclerotic aortic arch aneurysm. Second, flow patterns and shear stresses are different between varying shapes of aortic cannulas, as we had previously reported. Using dispersion-type cannula in our present model, we found large vortices in the transverse arch on longitudinal sections and dual clockwise vortices in the

horizontal sections. We suppose these vortices contributed to increased velocity fluctuations and strain rate tensors near the arch branches, in comparison with a normal aortic arch model. Third, the interaction between cannula stream and a complicated arch anatomy has been depicted three-dimensionally. In the AAA model, direct flow colliding with the ascending aortic wall may affect atheroma detachment, due to a higher shear stress in comparison with a normal aortic arch model. In addition, vortical flow may carry atheromatous material into the arch vessels more easily than in a normal model. Although turbulent flow near the arch vessels increased, shear stress on the aneurismal wall was smaller both in the Dispersion and the Soft-Flow cannula.

The Soft-Flow cannula is characterized by a series of lateral blowing jets from four side holes, contributing to a reduced sandblasting effect. It results in lower exit forces and flow velocities. In this study, there was marked attenuation of exit flow velocity, whereas shear stress remained unchanged. As previously reported though, exit flows can reach the posterior wall of the ascending aorta without attenuating its high velocity, thereby disrupting atheroma from the aortic wall.

Gooters et al. analyzed the flow from the cannula jet using intraoperative transesophageal echocardiography. They suggested that the dispersion cannula significantly reduced exit velocity. It was superior to the Soft-Flow cannula, as jets from the skewed-open side hole had the potential to disrupt plaque deposits along the posterior wall of the ascending aorta (Grooters RK. 2003). In our study, exit flow from the Dispersion cannula streamed along the posterior wall of the ascending aorta and inner curvature of the aortic arch. Therefore, we deduced that shear stress on the ascending aorta was smaller with a Dispersion cannula than with a Soft-Flow type. However, shear stress on the arch was high, particularly on the inner curvature of the aortic arch where plaques tend to localize in the elderly population or in patients with thoracic aortic aneurysm.

Limitation of the study

There are limitations to this study. The site and direction of cannula insertion may

have an effect on outcome. Certainly, if the cannulation site was positioned more proximally or distally in the ascending aorta, the streamline pattern and distribution of Urms values or strain rate tensors would vary. However, the exit flow velocities of the Dispersion and the Soft-Flow cannula attenuate within 4 to 5 cm from the exit site, so the shear stress at the aneurismal wall will not increase if aortic cannulas are placed in the ascending aorta. In contrast, if cannulas are placed in the proximal aortic arch, the sandblasting force would have an effect on the aneurismal wall, regardless of cannula type.

Conclusion

According to our observations, we should avoid using end-hole type cannulas in elderly patients with aortic arch aneurysm. Dispersion and the Soft-Flow cannulas are preferable to use in the atherosclerotic aorta, and great care should be taken in choosing the cannulation site and insertion angle because these cannulas have the potential of injuring ascending aortic plaques.

Section 3. Axillary perfusion in a normal and a AAA model

In "shaggy aorta" syndrome, manipulation of the ascending aorta may cause deleterious atheroembolism; therefore, it should be avoided. Retrograde perfusion from the femoral artery may induce "reverse" atheroembolism to the brain when patients have iliac artery atherosclerosis, abdominal aortic aneurysm and descending aortic aneurysm. Although the axillary artery perfusion is one of the solutions for this problem, there are several limitations for this method. Furthermore, detailed flow dynamics of the axillary artery perfusion had not been elucidated.

In this section we conducted in vitro investigations for axillary artery perfusion to clarify the hemodynamic effects upon the diseased aorta.

Materials and methods

A normal and a AAA glass aortic models were used. Detailed method of model making was described in the section 1. Conditions of perfusion was set same as previous experiment.

Results

Normal aortic model

In the right axillary artery perfusion model, rapid flow ran out from the BCA and grazed along lesser curvature of the aortic arch (Fig. 17). The maximal flow velocity on the BCA reached 80 cm/sec. The streamline divided into two directions: one went back to the aortic root along the lesser curvature of the ascending aorta making a secondary reversible vortex in the major curvature; the other descended along the lesser curvature of the aortic arch to the descending aorta making slow, helical flow in the descending aorta. In the left axillary artery perfusion model, rapid flow ran out from the ostium of the left axillary artery and directly went down into the descending aorta (Fig 18). Maximal flow velocity, as rapid as 78cm/sec, was observed around the ostium of the left subclavian artery. Secondary large, reversed vortex appeared in the transverse arch and tertiary vortex was observed in the ascending

aorta. Although flow in the aortic arch near the BCA was very slow, the streamline was very complicated. Magnitude of strain rate tensor, which is a function of the shear stress, was high on the ostium of the BCA and the LSCA (Fig 19).
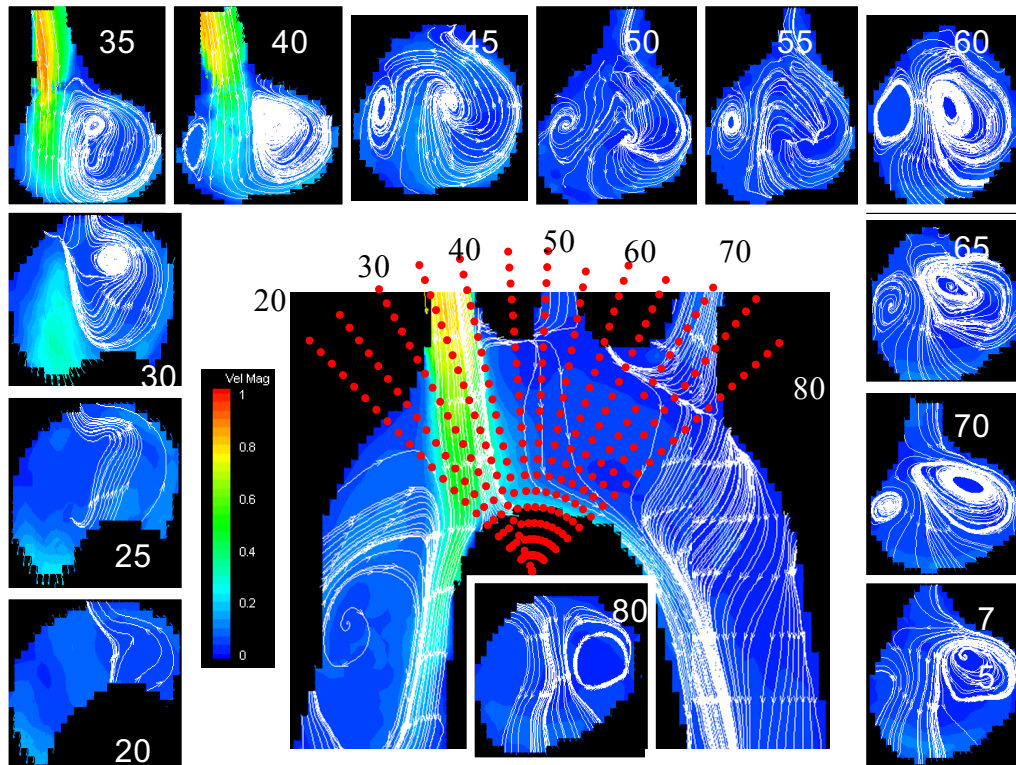
Fig. 17. Streamline mapping of the right axillary artery perfusion in normal aortic arch model.
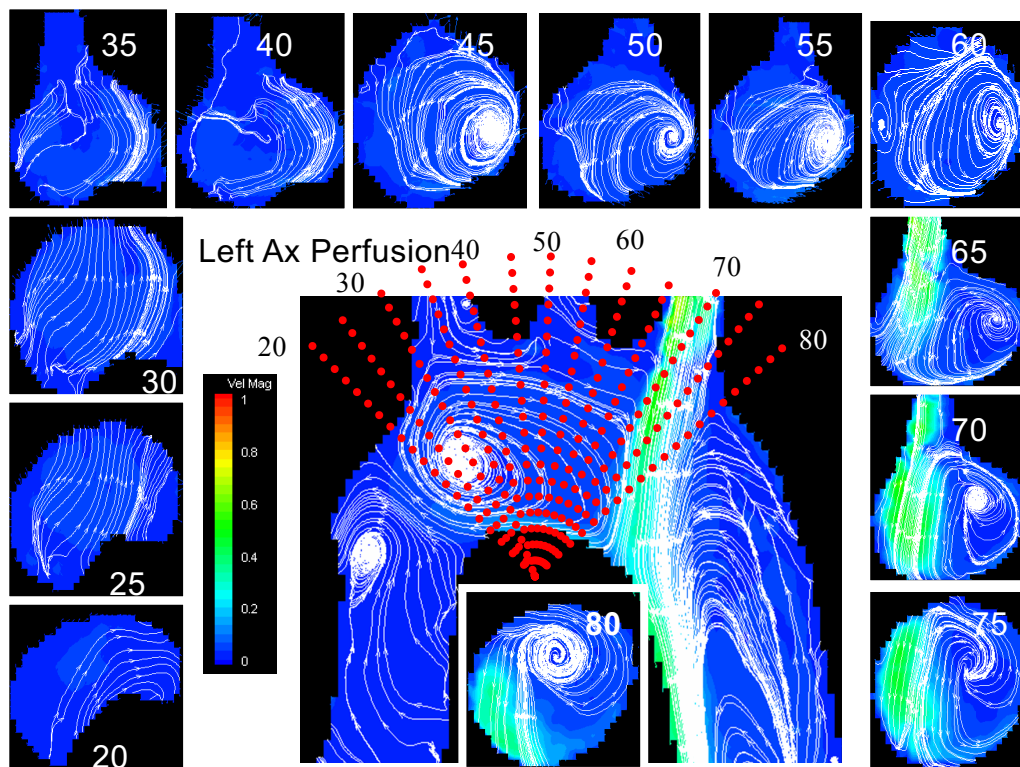
Fig 18. Streamline mapping of the left axillary artery perfusion in normal aortic arch model.
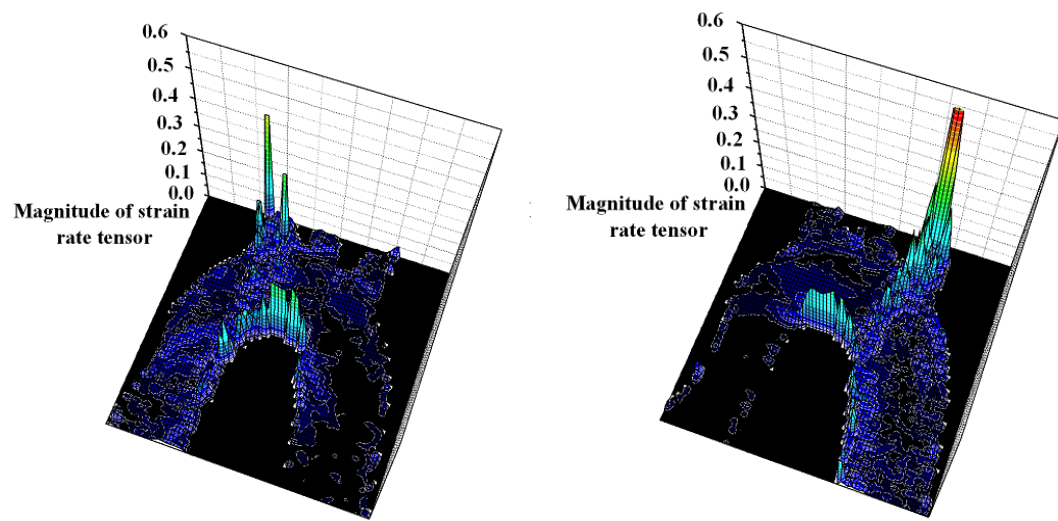
Fig 19. Distribution of the magnitude of strain rate tensor in the right axillary perfusion (left) and the left axillary perfusion (right) in normal aortic model

Aortic aneurysm model

Different from the normal aortic model study, aortic arch vessels are deviated proximally to the ascending aorta and the angle between the arterial outlet and the ascending aorta was obtuse. The flow from the BCA ran toward the posterior wall of the proximal aortic arch directly without deceleration and hits the lesser curvature. Retrograde flow was seen from the proximal aortic arch into the ascending aorta. Secondary, reversed vortical flow went distally into the left common carotid artery and the descending aorta (Fig 20). Distribution of magnitude of strain rate tensor and turbulence was high along the BCA and the lesser curvature of the ascending aorta. In the left axillary artery perfusion model, flow from the left subclavian artery ostium ran toward the ascending aorta (Fig 3). Rapid flow and large shear stress were observed along the LSCA and the posterior wall of the ascending aorta opposite to the LSCA ostium.
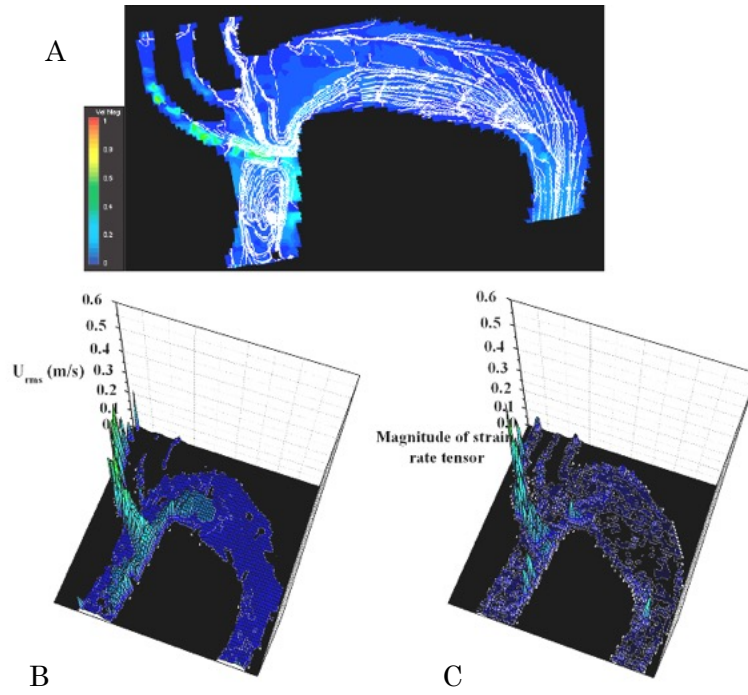
Fig 20. A. Streamline analysis of the right axillary artery perfusion in the aortic arch aneurysm model (top). Note rapid flow from the BCA hit the lesser curvature of the aortic arch. B. Distribution of the rms, representing degree of turbulence, is depicted in the right bottom plate. C. Distribution of the magnitude of strain rate tensor, function of the shear stress, is depicted in the left bottom plate.
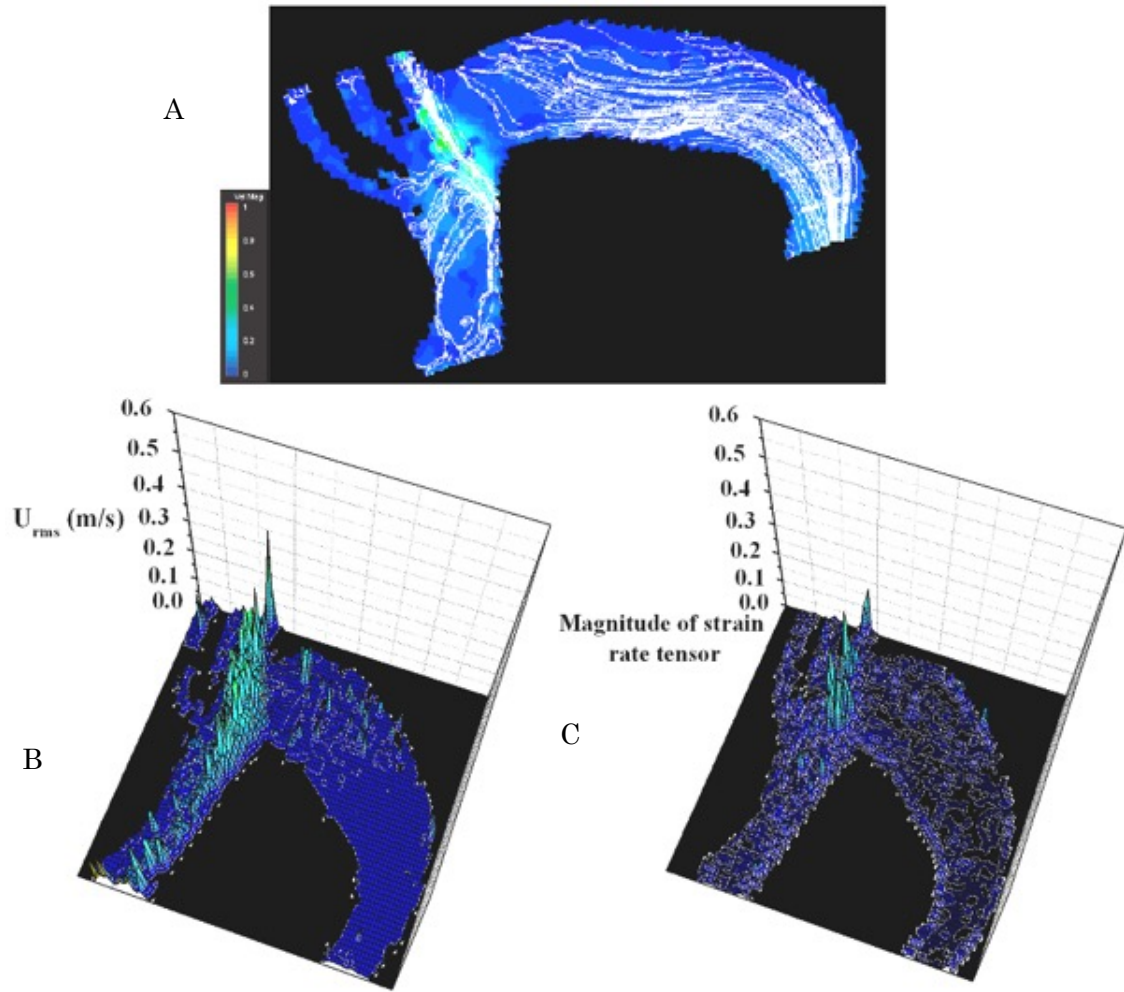
Fig 21. A. Streamline analysis of the left axillary artery perfusion in the aortic arch aneurysm model (top). B. Distribution of the rms, representing degree of turbulence, is depicted in the right bottom plate. C. Distribution of the magnitude of strain rate tensor, function of the shear stress, was depicted in the left bottom plate.

Discussion

Axillary artery perfusion had become popular as an alternative route to access the severe atherosclerotic aorta (Sabik JF. 1995)(Baribeau YR. 1998). The axillary artery perfusion is considered to be less invasive for patients with extensive atherosclerotic aorta (Kokotsakit J. 2005)(Okano M. 1993). The advantages of axillary artery perfusion are less likelihood of stroke from embolic material, less likely malperfusion with aortic dissection, and less disruption of atheroma. Svensson and colleagues analyzed 1352 operations with circulatory arrest for incidence of stroke from a standpoint of arterial cannulation sites (Svensson LG. 2004). They concluded that axillary artery cannulation with side graft was superior to the aortic cannulation and femoral cannulation to avoid stroke and hospital death by propensity analysis. The axillary artery perfusion is considered to promote antegrade flow to the aortic arch and the arch vessels. We had also used axillary artery perfusion as efficacious alternative site for patients with diffuse atherosclerosis of the aorta. However, there are several problems in this method. Anatomically, the diameter of the axillary artery is small especially in patients with delicate constitution. The effect of the jet flow from the orifice of the BCA or the left subclavian artery is not known clearly. Although it brings antegrade flow to the descending aorta, flow in the aortic arch may be turbulent and complex.

This study was conducted to evaluate the flow dynamics of the axillary artery perfusion model. The lesson from this study is that flow from the BCA in the right axillary artery perfusion goes toward the lesser curvature of the proximal aortic arch. Because the deposition of cholesterin to the aortic wall is prevalent on the inner curvature of the brachiocephalic ostium due to flow stagnation, shear stress caused by retrograde rapid flow from the axillary artery perfusion may detach the frail plaque. The important finding was that flow from the axillary artery did not spread homogeneously from ostia of the BCA or the LSCA into the aortic arch as surgeons have always imagined. Although the sandblast effect of the jet flow to the aortic wall is not well understood, we should be careful if the patient has frail or mobile plaque in the aortic lumen.

From rheological and pathological observation, orifices of arch vessels tend to have dense deposition of atheromatous plaque, which is observed as paste like material spilling out from the arterial wall during surgery. Sometimes patients have mobile, fragile plaque around the ostium of the BCA. This is caused by time averaged stagnant flow in the lesser curvature of the artery and increased permeability of the endothelium (Okano M. 1993). Theoretically, shear stress to the arterial wall increases proportional to shear velocity and viscosity. Flow velocity, which is proportional to shear stress, is governed by the length and diameter of the tube according to Poiseuile's equation. The route from the axillary artery to the ascending aorta is long and curved, so the effect of accelerated flow from the arterial orifice to the aortic wall is not known. Segadal et al. evaluated normal flow velocity in the ascending aorta in cardiac surgery patients using Doppler ultrasound probe. They reported peak forward flow velocity in the ascending aorta ranged from 45 to 67 cm/sec in coronary heart disease patients with normal aortic valve (Segadal L. 1987). They demonstrated skewed flow pattern, with oscillation during systolic-diastolic cycle in the mid-portion of the ascending aorta. Mean velocity and time averaged velocity in the ascending aorta in normal aortic valve patients was as low as 4.0 to 5.7 cm/sec and 6.8 to 13.5 cm/sec, respectively. Flow velocity in the aortic arch at 3 cm from the cannula exit in dispersion type cannula was 90 +/- 36 cm/sec. In our clinical study, flow velocity in the right axillary perfusion was as rapid as 159 and 201 cm/sec at the mid-portion and distal portion of the ascending aorta. Kvitting and colleagues reported peak velocity in the aortic root was 120 cm/sec using phase-contrast magnetic resonance imaging technique (Kvitting JE. 2004). Because pump flow is steady, time averaged flow velocity is very large compared to the pulsatile, natural flow in the normal aorta. In this study, flow velocity and shear stress were high at the ostium of the BCA and LSCA not only in the mock aneurysm model but also in the clinical study. Accelerated flow went proximally to the ascending aorta and it turned back toward the major curvature making a secondary slow, reversal vortex. Therefore, care should be taken when applying the axillary artery perfusion to the patients having frail atheroma on the posterior wall of the

ascending aorta or around arch vessels. Diversity of the aortic configuration and flow characteristics by each arterial perfusion should be considered to decrease morbidity of atheroembolic stroke and other embolic complication when patients with extensive atherosclerosis undergo cardiac surgery. Case by case approach and determination of arterial access may be appropriate strategy to prevent atheroembolism.

Limitation of the study.

We tested only one type of aortic arch aneurysm model. However, we regard the most important point is the angle between these arch vessels and the aorta. The lesson from this study is that flow from the axillary perfusion was not so soft. There was no side branch (the right common carotid artery) in the right axillary perfusion model. We concluded it would not significantly affect flow dynamics because the flow rate to the right carotid artery is small enough to ignore (Gerdes A. 2000).

Conclusions

Flow in the aortic arch and the ascending aorta was unexpectedly rapid and heterogeneous in the axillary perfusion model study. Special care must be taken when the patient has frail atheroma around arch vessels or lesser curvature of the aortic arch in the axillary artery perfusion.

Section 4. Apical aortic cannulation

Transventricular aortic cannulation is one of the alternative arterial accesses in surgery for diseased aorta, such as acute type A aortic dissection and extensive atherosclerotic thoracic aorta (Flege JB. 2001)(Wada S. 2006)(Fukuda I. 2002). It is also useful in surgery for descending aorta involving distal aortic arch through a left thoracotomy (Shiiya N. 1997). Several case reviews of this approach were reported. The advantage of this method is prevention of malperfusion by avoiding retrograde perfusion from the femoral artery and preventing atheroembolism by avoiding manipulation of diseased aorta. However, flow dynamics of this approach is not clear. The objective of this study is to evaluate flow patterns of transventricular aortic cannulation in the ascending aorta and the transverse aortic arch.

Materials and methods

Aortic arch model

The normal aortic glass model was used. The cannula was inserted from the aortic root (the proximal stump) of the glass model. of the glass model. The tip of each cannula was positioned at 2 cm above the aortic valve. Conditions for perfusion was same as section 1.

Aortic cannula

We tested three aortic cannulas in this study. Cannula A, Toyobo wire-reinforced 7mm venous drainage cannula (Toyobo, Co., Osaka, Japan) has four side holes and one end hole. Flow from cannula A goes out mainly from the small end-hole and tributary streams go out through the side holes in wide angle (Fig. 20-A). Cannula B, Toyobo 7mm apical aortic cannula is a newly designed transventricular aortic cannula which has cage shape pentagonal septa with a small end-hole. Flow from cannula B makes candle-flame-shape flow (Fig. 20-B). Cannula C, 7 mm Sarns Soft-Flow model CV4948, (Terumo Cardiovascular System Co., Tokyo Japan) has an oblique head and a cone shape flow splitter with torpedo-tube-shape exits (Fig. 20-

C). Flow from cannula C goes in four directions with separate angle. In this experiment, sharp tip of the cannula C was positioned toward the lesser curvature.

Visualization of flow pattern

Visualization of perfusate in the aortic arch model was performed by PIV method as shown in the section 1. Data were compared with standard aortic cannulation using 7 mm Sarns Soft-flow model CV 5767 (Toyobo, Co., Osaka, Japan) in previous experiment. In contour mapping of magnitude of flow velocity, strain rate tensor and turbulence, averaged power of vectors in each short axial plane was depicted in longitudinal map.

Results

Streamline of three cannulas in longitudinal and short axial plane is shown in figures. In cannula A, flow velocity near the exit was as fast as 0.9 m/sec and rapid jet flow was observed up to 40 mm from the tip of cannula (Fig. 21, 22A). Then flow velocity decreased gradually. Streamline analysis showed slow steady flow in the aortic arch with small retrograde vortex. Magnitude of flow velocity contour map demonstrated linear velocity peaks continued to the proximal aortic arch. Because area of the most rapid flow at the cannula exit was very small, maximum averaged-flow-velocity in contour mapping was expressed lower compared to the longitudinal flow map. In cannula B, the most rapid flow appeared around the cannula tip and the maximal velocity was approximately 0.7 m/sec. However, flow decelerated within 20 mm from the exit (Fig. 22B and 23B). Streamline analysis revealed steady streamline in the ascending aorta. In cannula C, distribution of the flow velocity was asymmetrical due to the asymmetrical shape of the cannula and maximal flow velocity area appeared only around the cannula tip. The flow was divided around the cannula exit (Fig. 22C). The maximal flow velocity was 0.4 m/sec, which appeared only around the cannula tip. Streamline analysis revealed steady and slow laminar flow without reversal of flow in the inner curvature of the aortic arch (Fig. 22C and 23C).

Distribution of the magnitude of strain rate tensor, which represents shear stress in the aortic lumen, is shown in Fig. 23. Magnitude of strain rate tensor decreased in the proximal ascending aorta in each cannula, but it was largest in cannula C. However, magnitude of strain rate tensor was smallest in cannula C. Comparing to the standard aortic cannulation, flow from apical cannulas generated steady, less turbulent and smaller shear stress in the aortic arch. Distribution of Urms (function of root mean square of velocity fluctuation) in each cannula is shown in Fig 24. It was large in cannula A and cannula B and maximal Urms was observed in the proximal ascending aorta. Urms decreased in the proximal arch in cannula A and B. On the contrary, maximum Urms was observed around the exit of the cannula but it was small in cannula C.
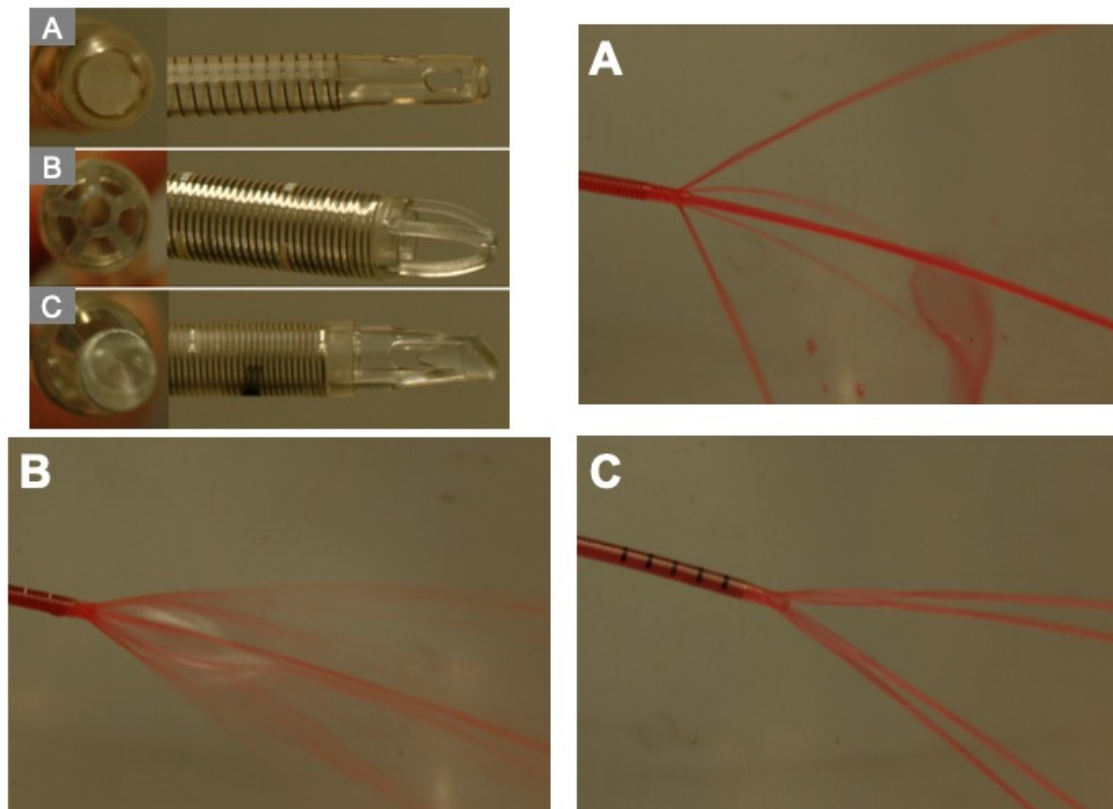
Fig 20. Shape of the tip in tested cannulae and flow pattern in the air. A: Toyobo wire-reinforced 7mm venous drainage cannula, B: Toyobo 7mm apical aortic cannula, C: 7.0mm Sarns Soft-Flow model CV4948
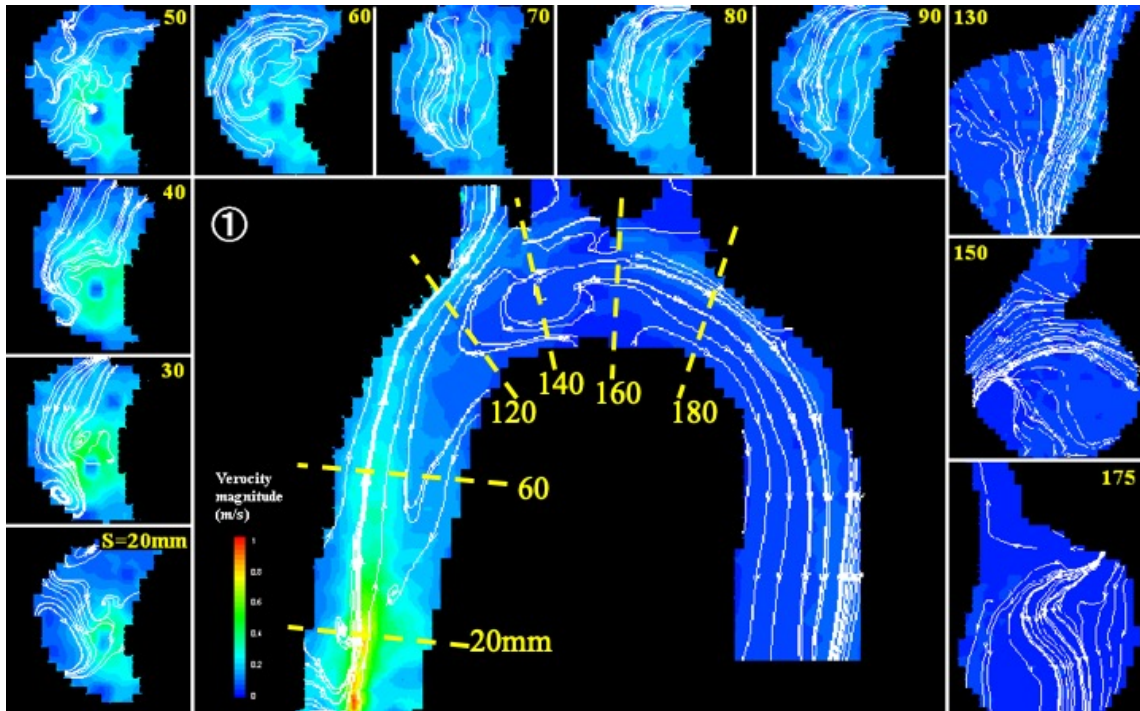
Fig 21.　Distribution of flow velocity mapping and streamline analysis of cannula A. Longitudinal view is shown in the center of the plate and cross-sectional view of the aorta in each level is shown in the surroundings. Flow velocity is depicted in color scale.
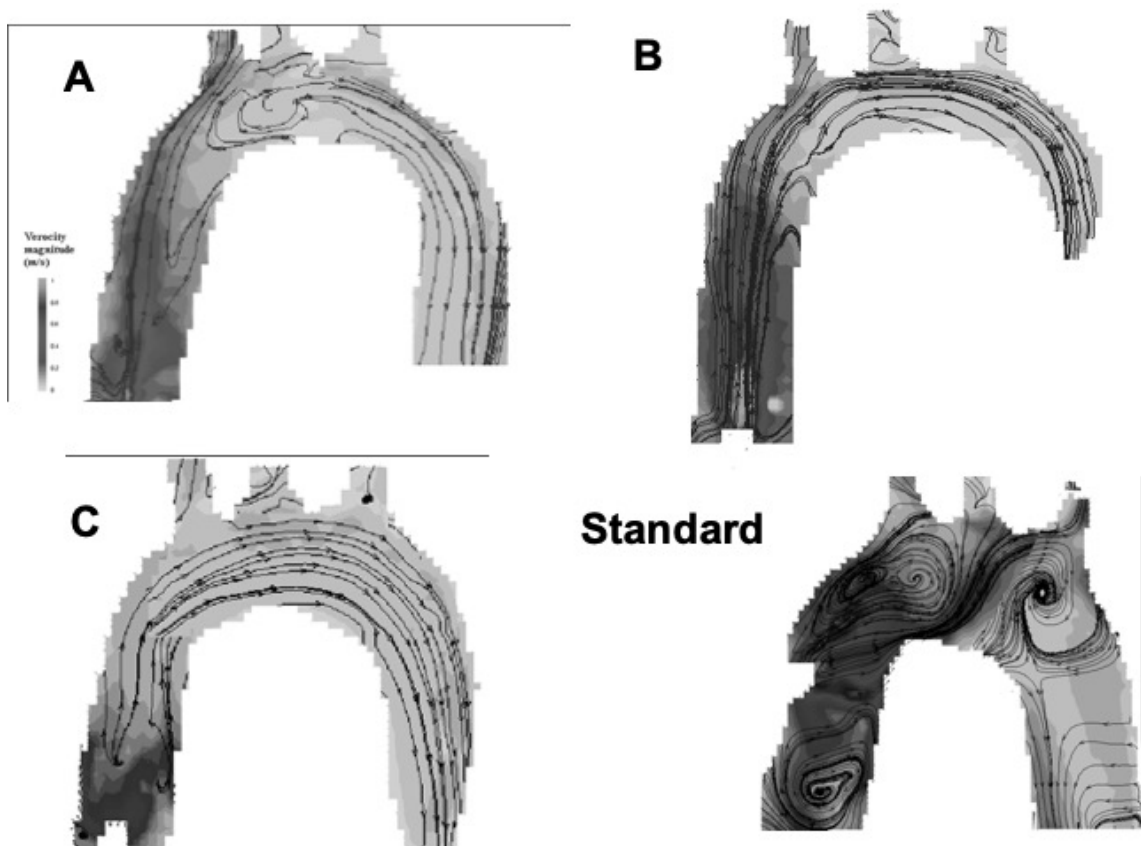
Fig 22. Streamline analysis of each cannula in longitudinal section.
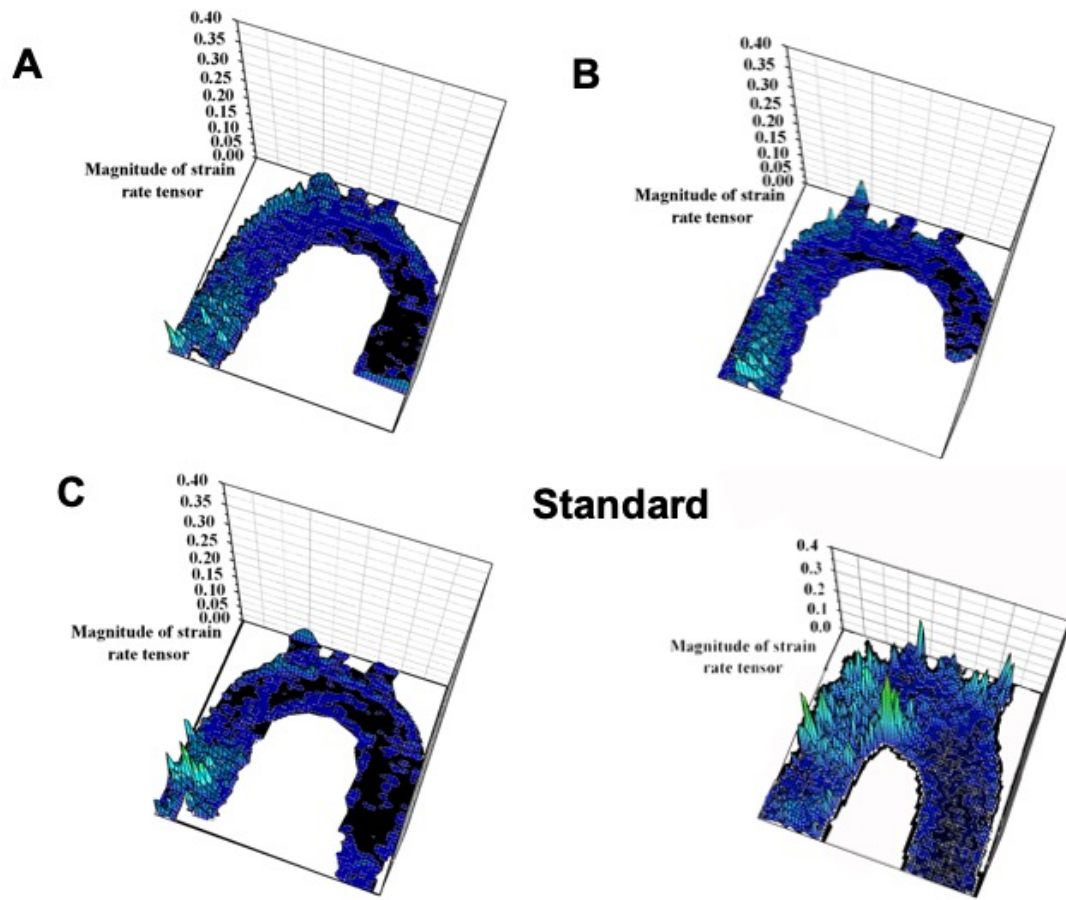
Fig. 23. Longitudinal mapping for distribution of magnitude of strain rate tensor in each cannula. Height of each wavelet expresses magnitude of shear stress.
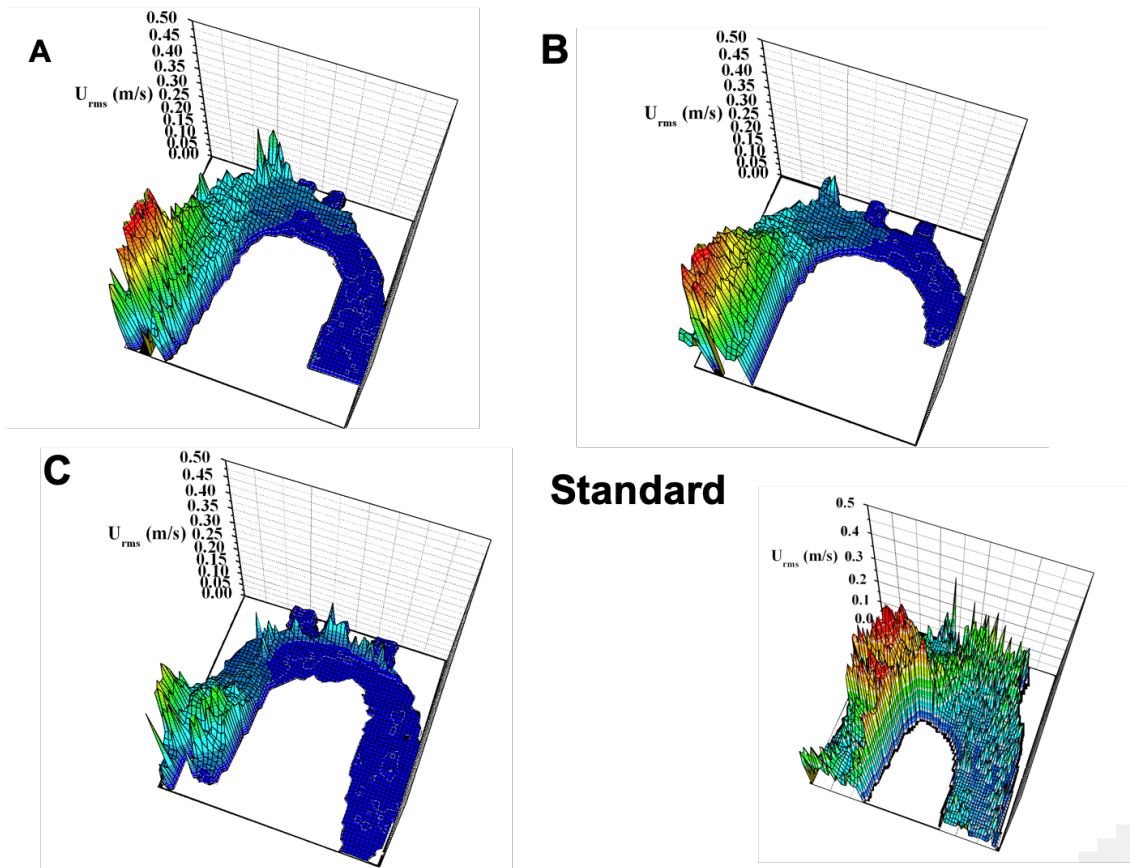
Fig. 24. Longitudinal mapping for distribution of Urms in each cannula. Height of each wavelet expresses degree of turbulence at each location.

Discussion

Previously analysis of the aortic cannulation in a glass model showed rapid jet flow from aortic cannula tip induced high shear stress and turbulence in the transverse aortic arch. Although sandblast effect of the arterial perfusion is not clearly understood, it is obvious that slow and laminar flow in the aorta is advantageous for cardiopulmonary bypass especially in aged patients with severe aortic atherosclerosis.

This study demonstrated that flow pattern in transventricular aortic perfusion was absolutely different from that in standard aortic perfusion from the ascending aorta. The evaluated cannulas had multiple outlets with complex shape to reduce flow velocity. Each cannula had characteristic flow pattern owing to position of the outlets and shape of flow splitter. The lesson from this study was that parameters of flow were mild in transventricular cannulation using these cannulas. Area of high shear stress was limited in the proximal ascending aorta. This means transventricular apical aortic cannulation can generate less invasive flow to the diseased aorta.

In pulsatile flow, cyclic flow requires larger maximal flow volume during systolic phase than constant flow (Segadal L. 1987). Therefore, a large aortic valvular area is necessary in the physiological situation. Although cross-sectional area of arterial cannula was smaller than natural aortic orifice, deceleration of flow velocity was prominent and we could obtain orderly streamline in the aorta. Constant flow from the small cannula may require smaller averaged flow resistance and the rapid jet from the cannula tip may be attenuated within several centimeters from the exit. Because dispersive type cannula tended to have decelerated flow velocity, shear stress in the ascending aorta was small. Generally, as atheromatous thickening and lipid deposit is mild in the ascending aorta, low shear stress generated by the jet flow is advantageous in surgery for patients having severe atheromatous change around the transverse arch.

The clinical problem in transventricular apical cannulation is bleeding from the left ventricular apex. Wada and colleagues reported safety and efficacy of

transventricular apical aortic cannulation under universal use for surgery of acute type A dissection (Wada S. 2006). They reported incidence of intractable bleeding due to transventricular cannulation was zero among 138 patients. Another concern for transventricular cannulation is aortic regurgitation induced by cannula insertion. In our clinical observation, aortic valve was competent in transventricular perfusion during ventricular fibrillation. Left ventricular venting from the right upper pulmonary vein or the left apex is necessary. Type B cannula is advantageous from the view point of left ventricular venting.

Limitation of the study

There were several limitations in this study. In aged patients, ascending aortic shape is more tortuous and curved than this model. Cannula tip cannot be positioned precisely in the center of the aorta in clinical situations. These problems will be solved in a computer-simulation model based upon our experimental data in the future.

Conclusion

Transventricular aortic perfusion generated slow and steady flow in simulated extracorporeal circulation model. It may be useful as an alternative cannulation site in surgery for patients with extensive atherosclerotic aorta.

Section 5. Aortic perfusion directing cannula tip directed toward the aortic root

   Sandblast effect caused by rapid flow from aortic cannula may play some role in atheroembolism in patients having atherosclerosis of the transverse aortic arch. DCT dispersion cannula (Edwards Lifescience LLC, Irvine, CA, USA, Fig 25) was designed to attenuate flow velocity making a fan-shaped flow by flat reflector. Grooters et al. reported efficacy of directing the DCT dispersion cannula toward the aortic valve to reduce atheroembolism during coronary artery bypass grafting (Grooters RK. 2000).   The objective of this study was to elucidate the rheology of the arterial cannula tip and effect of cannula tip direction

Materials and methods

Aortic arch model and visualization of flow pattern

   The normal aortic glass model and AAA glass model were used in this study. Detailed method of glass model reconstruction was described in our previous section. We analyzed the flow of DCT21A dispersion cannula in two directions; standard aortic cannulation directing the cannula tip toward the aortic arch (standard direction) and the other was modified cannulation with the cannula tip directed toward the aortic root (root direction). Flow in normal aortic model and aortic aneurysm model was evaluated.
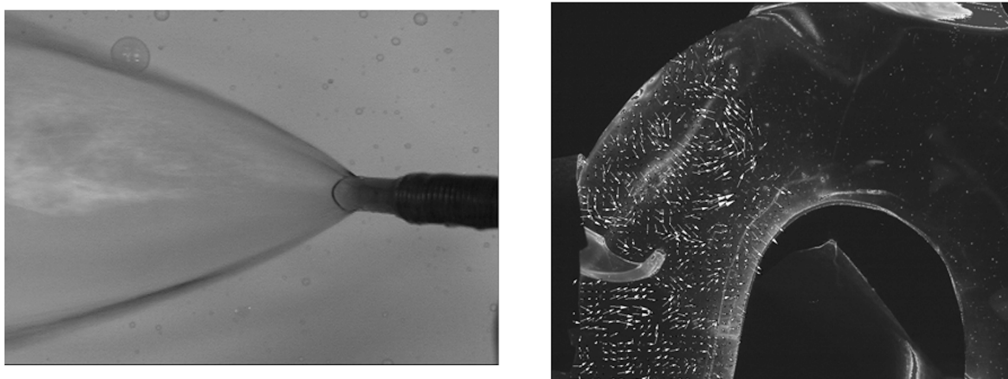

Fig 25. Dispersion cannula (left) and glass normal aortic model (right)

Quantitative analysis of flow vectors

Velocity magnitude of flow vectors was measured at 75 points in each cross-sectional plane of the aortic model in normal aortic model. Absolute values of average, maximum, and minimum flow velocity vectors in each cross-sectional plane were depicted according to distance from cannula tip. Because cross-sectional areas were heterogeneous, this comparison was not performed in aneurysm model.

Results

Flow analysis in normal aortic model.

When cannula tip was positioned to standard direction, vortical regurgitant flow was observed on the greater curvature side of cannula near the ostium of the BCA. Adjunctive vortex appeared in the distal aortic arch. Because the flow ejecting from the dispersion cannula spreads out in a fan-like form on the plane perpendicular to the two-dimensional projection, streamlines ejecting away from the cannula tip were not clearly depicted in the streamline map in the longitudinal plane. Magnitude of flow velocity in the aortic arch was faster in standard direction than that in root direction (Fig 26). When the cannula tip was directed toward the aortic root, streamlines formed complicated vortexes indicating two directional flow streams ejected from the cannula tip and reflected by aortic root (Fig 26). Velocity distribution revealed fast flow toward the aortic root but very slow flow in the aortic arch. Points of high shear stress appeared along the greater curvature and in the proximal portion of the lesser curvature in standard direction (Fig 27). Although shear stress was high in the ascending aorta in root direction, it was low in the transverse aorta. In standard direction, distribution of Urms was relatively homogenous. In root direction, distribution of Urms was high in the ascending aorta reflecting diverse direction of flow vectors. However, distribution of Urms in the transverse aorta was uniformly low in root direction (Fig 28).

Flow analysis in the aortic arch aneurysm model

In the aortic arch aneurysm model, streamline analysis in standard direction demonstrated complicated flow in the transverse aorta. Rapid flow velocity area and regurgitant vortex was observed around aortic arch vessels in longitudinal plane. Regurgitant streamlines grazing the lesser curvature finally went back into arch vessels. In cross-sectional plane, two reversely directed vortexes gushing out from the lesser curvature were observed at 40 mm from the cannula tip, where arch vessels arose (Fig. 29). Magnitude of velocity vectors in this area was large. On the other hand, flow velocity in the aneurysmal region was slow. In root direction, rapid flow was observed in the aortic root region. However, flow velocity map demonstrated generally slow flow distribution around the aortic arch vessels and in aneurysmal region. Two reversely directed vortexes in the arch vessel area were observed in cross-sectional plane at 40 mm, but velocity vectors were smaller than that in standard direction.

In shear stress analysis, high |D| value area was observed in cannula tip, ostium of the brachiocephalic artery and the roof of the aneurysm in standard direction (Fig 30). In root direction model, high |D| value area was observed in the transverse aortic arch.

Quantitative analysis of flow vectors in normal aortic model

Absolute value for flow vectors in cross-sectional component was compared in standard direction and aortic root direction (Fig 31). Although range of absolute value of the flow vectors was high in the ascending aorta in root direction, that in the transverse aorta was low in comparison with standard direction model.

61

Fig 26. Streamline and flow velocity analysis of two directions in normal aortic model. a: standard direction, b: root direction. Flow vector map in cross-sectional plane is shown in the surrounding schema. Cross-sectional vector analysis is shown on right plates. c: enlarged view of streamline and flow velocity distribution in the aortic root in cannula tip directing the root. Flow velocity is depicted with color scale grading. Yellow arrow indicates cannulation site and direction of cannula tip.

Fig 27. Distribution of shear stress, |D|, in the ascending and transverse arch in normal aortic model. a: standard direction, b: root direction. Black arrow indicates cannulation site and direction of cannula tip.
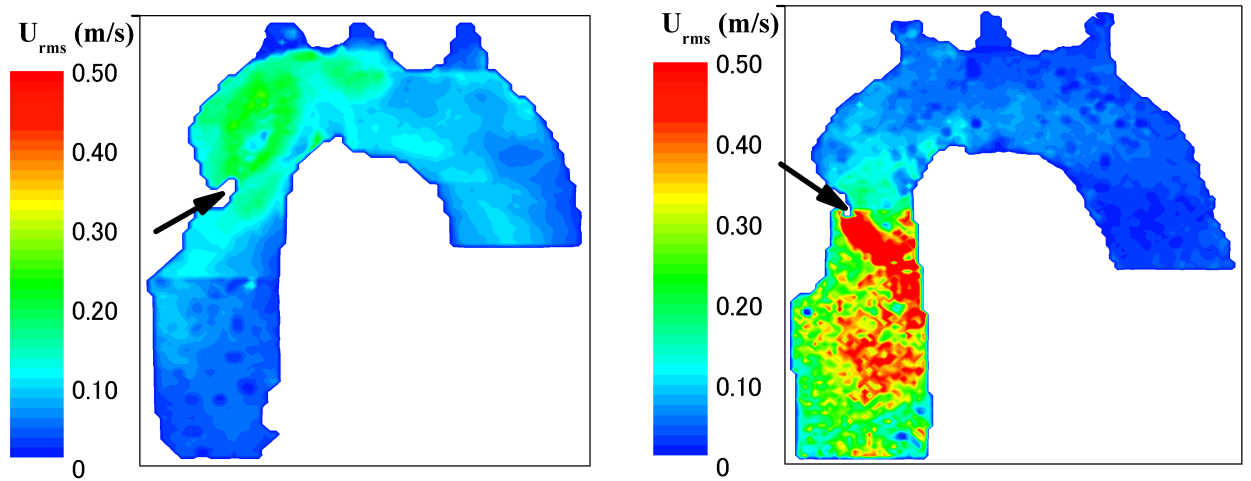
Fig 28. Distribution of turbulence, Urms, in cannula tip directing toward the aortic arch (left)　and in cannula tip directing toward the aortic root (right)
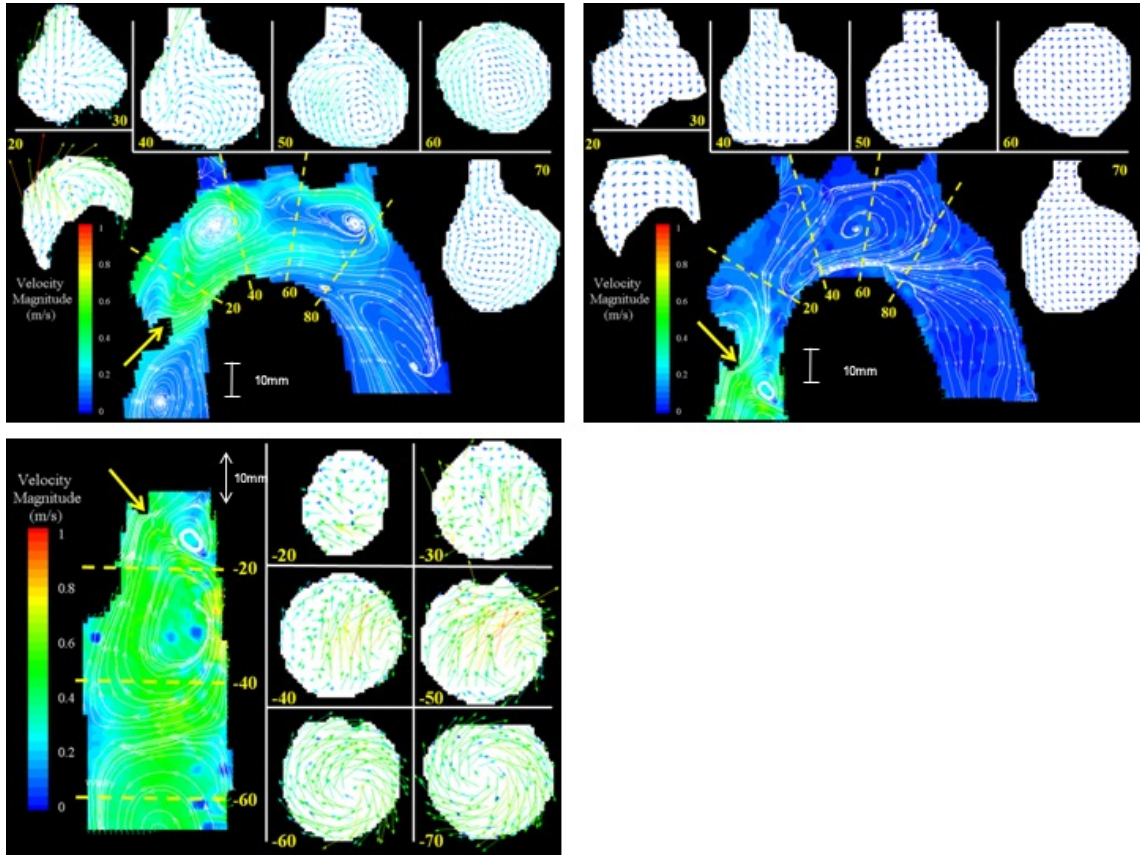
Fig 29. Streamline and flow velocity analysis of two directions in AAA model. a: standard direction. b: root direction. Flow vector map in cross-sectional plane is shown in the surrounding schema. Magnitude of velocity vector component is expressed in color and length of vector arrow. Yellow arrow indicates cannulation site and direction of cannula tip.
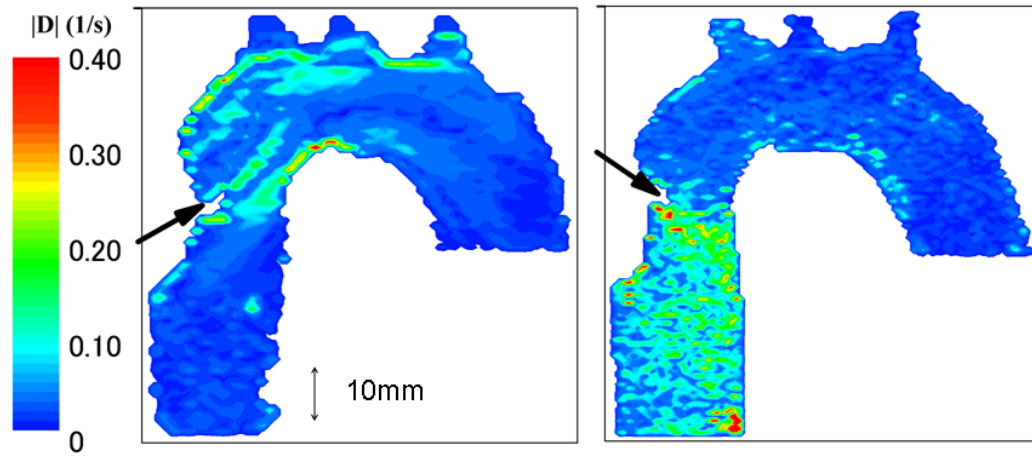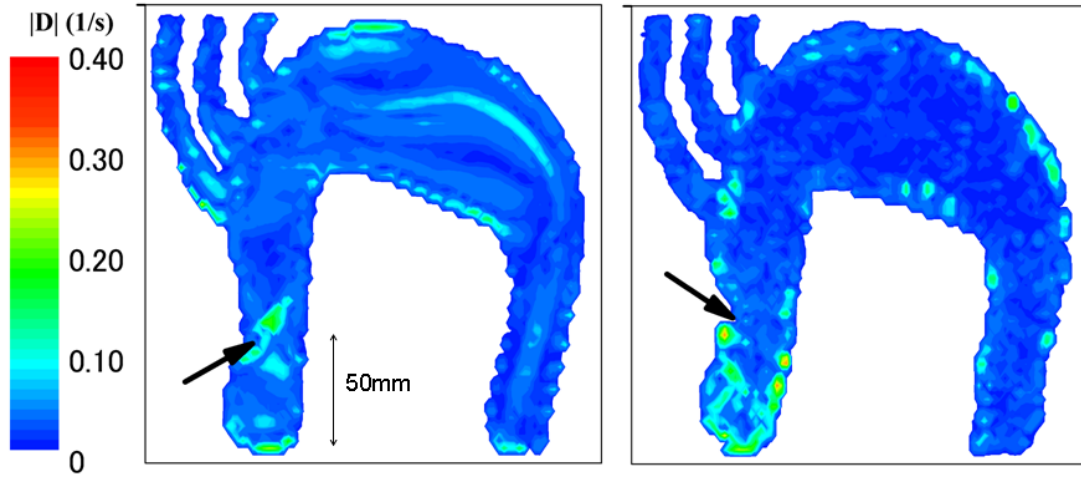
Fig 30. Distribution of shear stress, |D|, in the ascending and transverse arch in aortic arch aneurysm model. a: standard direction, b: root direction. Black arrow indicates cannulation site and direction of cannula tip.
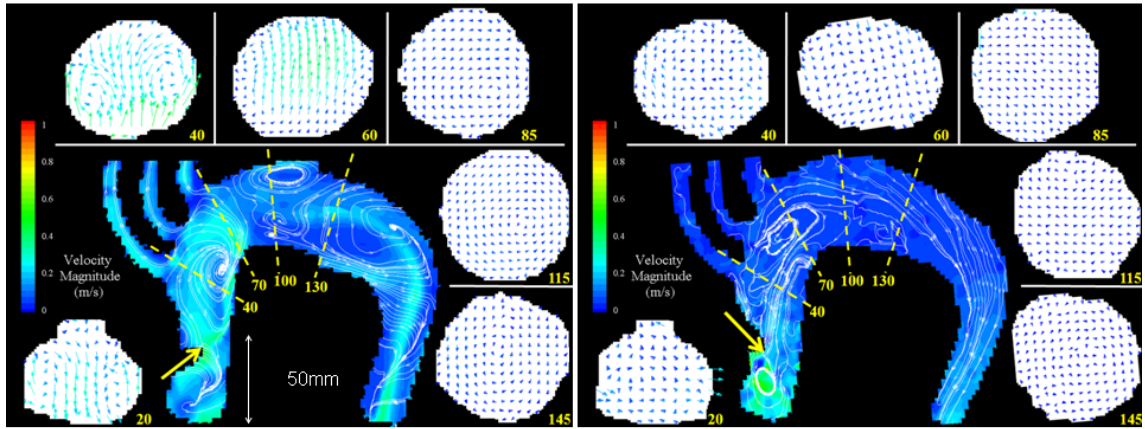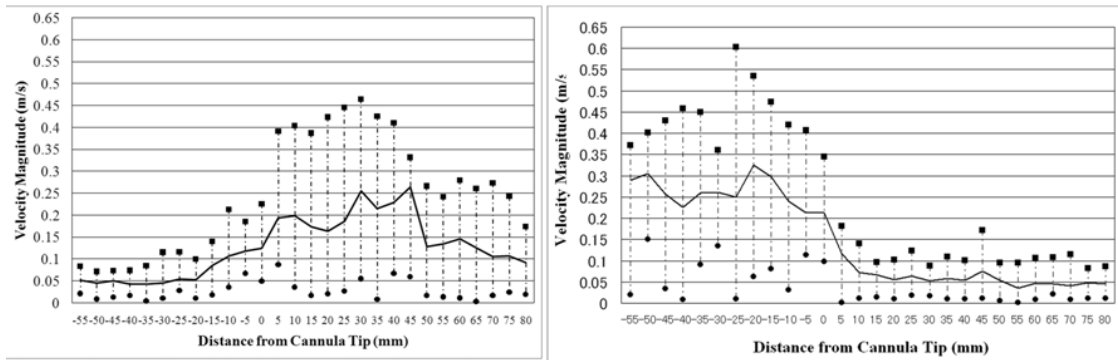

Fig 31. Flow velocity vector distribution in each cross-sectional area. Point 0mm indicates cannulation site. Absolute value of velocity magnitude vectors in each cross-sectional plane is depicted along distance from cannulation site. Dotted bars indicate range of vector value. Average value is connected by real line. Minus sign indicates direction toward aortic root along longitudinal axis of the aortic model. Left: standard direction, right: aortic root direction.

Discussion

Recently, more aged patients are undergoing cardiac surgery using CPB for ischemic heart disease, thoracic aortic aneurysm, and degenerative valvular disease.

65

As patients' age advances, prevalence of atherosclerosis of the ascending aorta and aortic arch increases. Sometimes cardiac surgeons encounter paste-like material filling in the aortic wall or frail atheroma in the ascending aorta and the aortic arch in surgery for the ascending aorta and transverse aortic arch (Wareing TH. 1992)(Ribakove GH. 1992). Djaiani and colleagues demonstrated correlation between embolic signal count in the area of the middle cerebral artery detected by transcranial Doppler during CPB and postoperative embolic stroke detected by diffusion-weighted magnetic resonance imaging (Djaiani G. 2004).

DCT dispersion cannula has unique shape with flat and obtusely angled flow reflector. It generates fan shaped flow without destruction of cellular components of blood. Flow velocity distribution in the transverse aorta in this experiment was almost same as an average flow velocity distribution in physiological condition (Segadal L. 1987). Owing to reduction of flow velocity and shear stress, directing DCT dispersion cannula toward the aortic arch is beneficial when flail atheromatous plaque exists in the distal aortic arch. However, when there is thick soft plague on the lesser curvature of the aortic arch, tangential shear force may displace and detach the protruding atheroma in the lesser curvature (Fukuda I. 2007). Streamline analysis in this study demonstrated reversely directed streamlines from the aortic arch went into arch vessels in normal and aneurismal models when the cannula tip was directed toward arch direction. Considering shear force distribution, detached debris may flow into the brain circulation following these streamlines.

Our experimental study proved that flow in the aortic arch was slow and less turbulent when the cannula tip was directed toward aortic root in either normal or aneurysm model. While shear stress was high in the ascending aorta, it was very low in the transverse aortic arch in this method. On the other hand, degree of turbulence was high in the ascending aorta when cannula was directed toward the aortic root.

Despite flow velocity reduction in the aortic arch aneurysm model, flow velocity and shear force were high in proximal aortic arch where cranial vessels arose. Reverse flow within the arch may induce atheroembolic stroke because severe

intimal change frequently exists around there. Therefore, aortic cannulation toward root direction is one of the options for surgery in patients having severe atherosclerosis of the transverse aortic arch. Because shear stress and turbulence are high in the ascending aorta, aortic root direction should not be used if there is calcified vegetation around aortic root in patients with senile aortic stenosis. Root direction is also contraindicated in aortic regurgitation due to high velocity magnitude distribution in the aortic root.

Limitations

There were several limitations in this study. The shape of the ascending aorta and the transverse aorta is diverse. Selection of aortic cannulation sites is limited by aortic morphology, surgical approach and operative field in clinical practice.

Conclusion

Directing DCT21A dispersion cannula tip toward the aortic root generated slower and less turbulent flow in the transverse arch of transparent aortic model in comparison with flow in standard directed cannulation. Sandblast effect caused by high velocity and shear stress from cannula tip may be attenuated in this method.

Section 6. Third-generation dispersive aortic perfusion cannula (EZ glide) directing toward the aortic arch and the aortic root

The Edwards Research Medical EZ Glide Aortic Perfusion Cannula ™ (EZG cannula, Edwards LifeSciences, LLC, Irvine, CA, USA) was developed to attenuate flow in the aorta and to avoid atheroembolism due to jet flow. Until 2014, the market of aortic cannula was shared by a first-generation end-hole cannula and second-generation dispersive cannulas (Soft-flow cannula; 3M Cardiovascular, Ann Arbor, MI, USA; and Dispersion cannula; Edwards LifeSciences, LLC, Irvine, CA, USA) in Japan (Fukuda I. Kyobu Geka. 2009). However, Soft-flow cannula was withdrawn from the market in accordance with instructions from the United States Food and Drug Administration in 2015.

In section 5, we showed that the dispersion cannula generates gentle flow in the aortic arch, especially when the cannula tip is directed toward the aortic root. The flow characteristics of EZG cannula have not been well characterized, especially when the cannula tip is directed towards the aortic root. The objective of this study was to evaluate the magnitude of flow velocity, distribution of shear stress and flow turbulence in the experimental aortic model using an EZG cannula.

Material and Method

Conditions of perfusion cannula

Three types of aortic perfusion cannula were tested: a non-dispersive curved end-hole cannula with a 45-degree angle (Toyobo Oukn-L-7.3-mm, Toyobo, Co., Ltd., Osaka, Japan), Dispersion cannula, and the EZG cannula. In Dispersion and EZG cannulas, flowmetry was performed with the cannula tip either directed toward the aortic arch or the aortic root (Fig. 32, 33). Flow velocity at the ostium of arch vessels was measured and compared in each cannula.

Fig 32. Edwards EZ glide cannula. The cannula tip is curved (45 degrees). Cannula exit creates a pentagonal outlet with the mainstream on the lesser curvature of the cannula tip. It creates flame-shape flow from the exit.
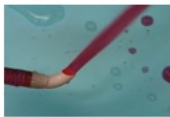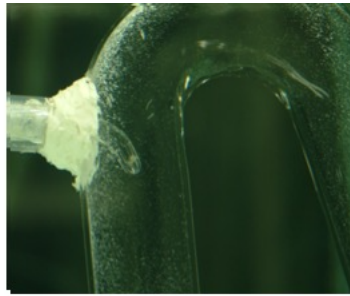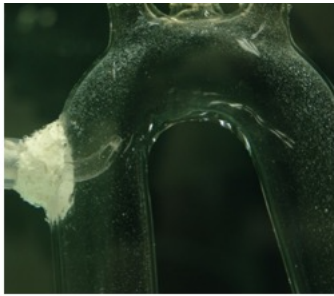
Arch direction
End-hole,
Dispersion,
EZ glide

Root direction
Dispersion, EZ glide

Fig 33. Experimental system. Left; Cannula tip is directed towards the arch. The end-hole cannula, the dispersion cannula, and the EZ glide cannula are tested. Right; Cannula tip is directed towards the root. The dispersion cannula and EZ glide cannula are tested.

Results

1)   *Flow velocimetry in the glass aortic model with the cannula tip directed towards the arch*

Flow from the end-hole cannula went straight to the greater curvature. Rapid flow, which was as fast as 0.9 m/sec, collided with the ostium of the arch vessels without deceleration (Fig. 34). After hitting the aortic wall, the flow decelerated, resulting in reversed vortical flow in the distal arch and inner curvature. Some streams regurgitated to the proximal arch and went into the left carotid artery. Steady flow was observed in the descending aorta. Turbulent flow and high peaks of magnitude of SRT were observed on the outer curvature of the aortic arch (Fig. 35).

When directing the EZG cannula tip toward the aortic arch, streamline analysis revealed flame-shaped flow from the cannula tip. The main streamline went to the mid-portion of the transverse aortic arch and the lesser curvature. Although the maximal flow velocity was approximately 1.0 m/sec, which appeared on the lesser curvature, the volume of the rapid flow area was small. Flow velocity decreased within 20 mm from the cannula exit. The maximal SRT area appeared on the lesser curvature of the aortic arch. Peaks of the magnitude of SRT on the greater curvature were lower than end-hole cannula (Fig. 35).

2) *Flow velocimetry with the cannula tip directed towards the aortic root*

Flow distribution in the transverse aortic arch when the EZG cannula tip was directed towards the aortic root is shown in Fig. 6. When the EZG cannula was directed toward the aortic root, flow velocity distribution in the transverse aortic arch was as slow as 0.1 m/sec, despite rapid flow around the cannula exit in the ascending aorta. Distribution of Urms was small in the transverse aortic arch when the EZG cannula tip was directed towards the aortic root.

3) *Flow velocity on the arch branches*

Maximum flow velocity at the ostia of major arch vessels in each cannula was measured. Both the dispersion cannula and the EZG cannula generated slow flow in the aortic arch ostia (Table 1).
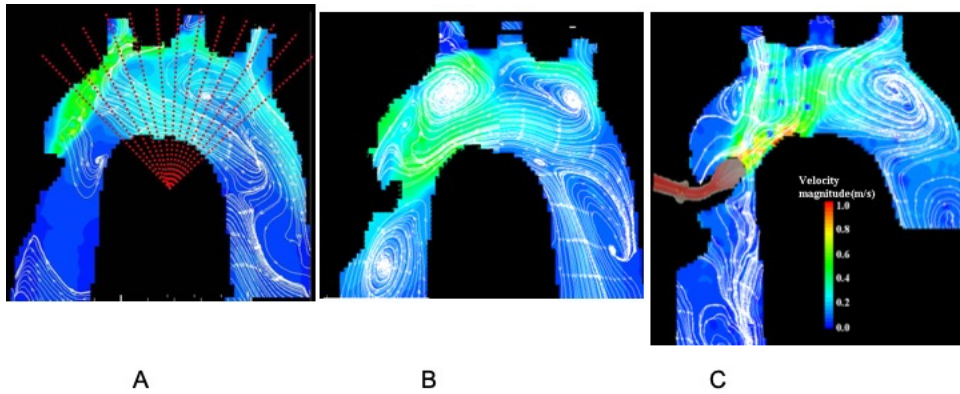
Fig 34. Streamline of cannulas directed towards the aortic arch. A; End-hole cannula, B; Dispersion cannula, C; EZ glide cannula. Flow distribution in transectional plane is obtained for each dotted section.
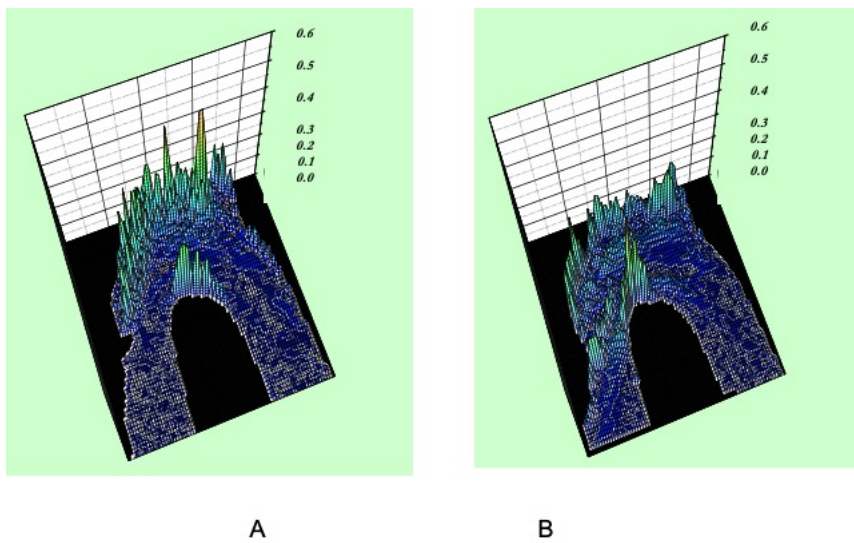
Fig 35. Distribution of magnitude of strain rate tensor, which is a function of the shear stress. A; End-hole cannula, B; EZ glide cannula. In the end-hole cannula, distribution of shear stress is great (Author: what do you mean by "great"?) along the greater curvature.　In the EZG cannula, maximal shear stress appears on the lesser curvature of the aortic arch.　With the EZ glide cannula, shear stress in the greater curvature is low.

A   B
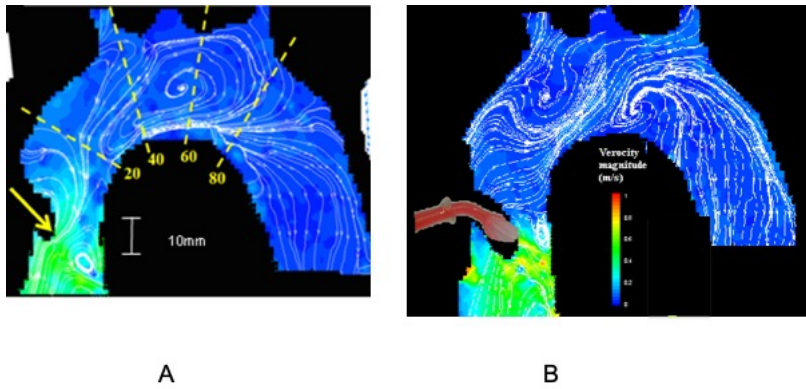
Fig 36. Flow velocity distribution and streamline in A; the dispersion cannula, B; EZ glide cannula with the cannula tip directed towards the aortic root.

Cannula \ Site	EH arch	Dispersion arch	EZG arch	Dispersion root	EZG root
Brachiocephalic artery	0.7	0.4	0.3	<0.1	<0.1
Left common carotid artery	0.5	0.2	<0.1	<0.1	<0.1
Left subclavian artery	0.35	0.2	0.3	0.1	<0.1

Table 1. Maximum flow velocity (m/sec) at the ostium of major arch vessels in each cannula. Flow velocity is showed in m/s. EH; end-hole cannula, Dispersion; the dispersion cannula, EZG; EZ glide cannula, arch; arch direction, root; root direction

Discussion

We previously demonstrated the efficacy of the Dispersion cannula when directed towards the aortic root in a mock glass aortic model. Those data showed decelerated flow in the aortic arch in Dispersion cannula when the cannula tip was directed towards the aortic root. In this study, we also showed a decreased flow velocity with the EZG cannula when compared with the end-hole cannula. When the EZG cannula is directed towards the aortic root, flow velocity distribution in the aortic arch was as slow as that with the Dispersion cannula. This is the first report to elucidate the flow characteristics of the EZG cannula when directing towards the aortic arch or the aortic root.

Conclusions

Flow from the EZG cannula was gentle when compared with that from the end-hole cannula when the cannula tip was directed towards the aortic arch. Shear stress is low along the greater curvature of the aortic arch with the EZG cannula. When the cannula tip was directed towards the aortic root, flow from the EZG cannula generated flow characteristics similar to those of the Dispersion cannula. The EZG cannula is an effective alternative to the Dispersion cannula with regards to flow characteristics.

Chapter 3. In vivo flow analysis during extracorporeal circulation

Section 1. Aortic perfusion

In Chapter 3, we will show clinical relevance to experimental data using intraoperative echocardiography.

Material and Methods

To clarify clinical relevance of sandblast effect from arterial cannulas, flow in cardiac operation using the extracorporeal circulation was investigated. Aortic cannulas were randomly allocated to two groups; 1) 21Fr Dispersion cannula (n=5), 2) Sarns Soft-Flow cannula (n=5). Because of high concern for atheroembolism in our study group, end-hole cannula was not used in clinical study. Written informed consent was obtained in each patient before operation. Aortic cannulation site was determined by information of preoperative CT scan and perioperative epiaortic echo. Patient demographics were not different between two groups. Intra-aortic flow analysis was performed using epiaortic echo and trans-esophageal echocardiography (TEE). Under the total perfusion at the flow rate from 2200 to 2400 ml/m2 with venting from left atrium, visualization of flow image by Color mode and measurement of maximal flow velocity (Vmax: m/sec) using epiaortic duplex scan were done at the level of aortic root, near the cannula exit inserted from ascending aorta (middle of the ascending aorta), proximal aortic arch and the middle aortic arch. Maximal flow velocity (Vmax: m/sec) by Doppler mode using TEE was measured at the level of distal aortic arch, descending thoracic aorta of pulmonary trunk level (middle descending aorta) and descending thoracic aorta of 10cm distal from pulmonary trunk level (distal descending aorta). Data was expressed by mean ± SD.
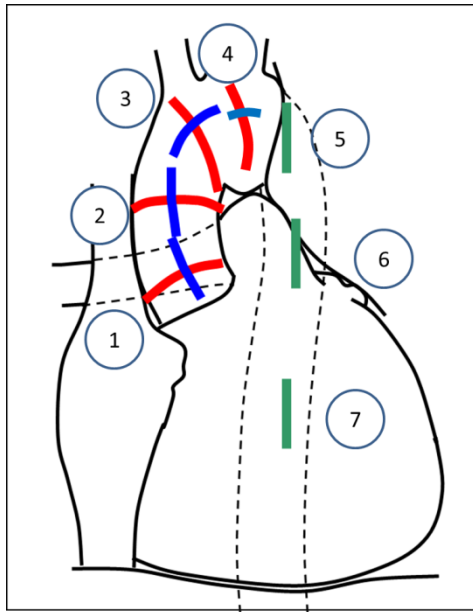
Figure 37. In vivo analysis of flow during extracorporeal circulation. ① .Proximal ascending aorta, ② Middle ascending aorta, ③ Distal ascending aorta, ④ Proximal aortic arch, ⑤ Middle aortic arch, ⑥ Distal aortic arch, ⑦ Middle descending aorta, ⑧ Distal descending aorta.

Results

In Dispersion cannula, fan-like shaped exit flow was streaming toward the inner curvature of the aortic arch. Turbulence with high velocity jet representing by mosaic echo pattern was not found at aortic root and outer curvature of the aortic arch where there are arch vessels (Fig.37). High velocity jet that the Vmax was 2.1 ± 0.9m/sec near the cannula exit decreased in middle arch to 0.8 ± 0.3m/sec. In descending thoracic aorta blood flow became almost steady flow at the velocity of 0.3 ± 0.1m/sec (Table 2.). In Soft-Flow cannula, four-directional dispersive jets from four skewed side hole were blowing toward aortic root, posterior wall of the ascending aorta and the proximal aortic arch. Flow velocity around the cannula tip ranged from 1.2 to 2.7m/sec, and turbulent flow shown by mosaic echo was found in the ascending aorta (Fig 38). However, high velocity jet was not reached in the middle arch where the cannula flow attenuated at the velocity of 0.7 ±0.5 m/sec. In descending thoracic aorta, blood flow became steady flow at the velocity of 0.2 ±0.1 m/sec (Table 2.).

	Asc Ao (m/sec)		Transverse arch (m/sec)			Desc Ao	
	Prox	Dist	Prox	Mid	Dist	Mid	Dist
DPS	1.1±0.4	2.1±0.9	1.3±0.9	0.8±0.3	0.4±0.3	0.4±0.1	0.3±0.1
SFT	2.7±1.9	1.5±0.9	1.2±1.0	0.7±0.5	0.8±0.3	0.6±0.4	0.2±0.1

Table 2. Flow velocity distribution in clinical cases. DSP; Dispersion cannula group, SFT; Soft-Flow group
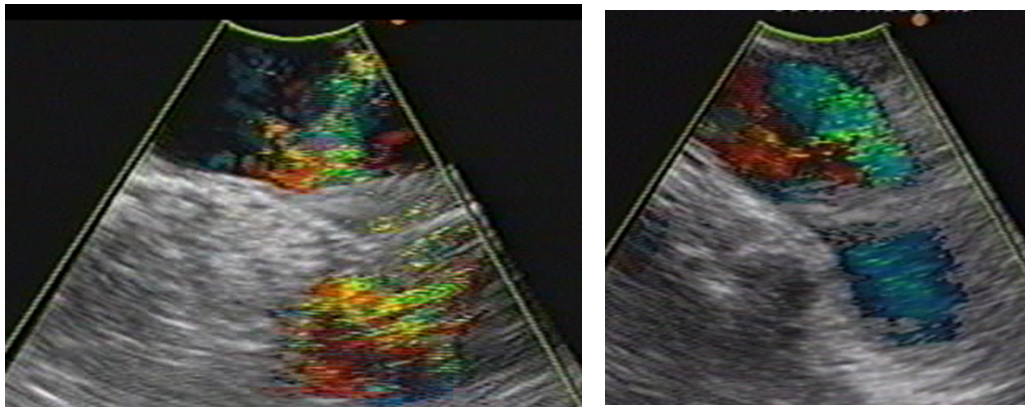
Figure 38. Flow pattern in the aortic arch from Dispersion cannula (left) and Soft-Flow cannula (right).

Discussion

In vivo experiment for flowdynamics of arterial perfusion is difficult because of morphological difference between experimental animal and humans. Porcine model is the most popular for medical experiment because of size and cost; however, morphology of the aortic arch is totally different between human and pigs. Therefore, model experiment and computed simulation is very important method for development of new technology in cardiac surgery.

Section 2. Axillary artery perfusion

In Chapter 2, we showed high velocity area appeared at the ostium of the BCA in the right axillary artery perfusion. In this section we will show clinical evaluation of axillary artery perfusion.

Patients and Methods

Intraoperative evaluation of the flow in the ascending aorta, the transverse arch and the descending aorta was performed during cardiac surgery using epiaortic echo and transesophageal echo in 3 patients. Indication for axillary artery perfusion was aortic arch aneurysm or ascending aortic aneurysm with diffuse atherosclerosis of the ascending aorta. The right axillary artery perfusion was employed because of our familiarity with this method in clinical practice. Dacron graft 8 mm in diameter was sewn to the axillary artery in end-to-side fashion and it was connected to the extracorporeal circulation circuit directly. Measurement of the flow characteristics was performed after establishing extracorporeal circulation without patient's own cardiac output with venting from left atrium. Perfusion index was maintained at 2.4 L/m2/min and perfusion pressure was maintained above 50 mmHg. Visualization of flow image by color mode and measurement of flow velocity using epiaortic echo and 7.5 MHz linear scan probe (SSD-5500 and UST-987, Aloka, Tokyo, Japan) was done at the level of the aortic root, the orifice of the brachiocephalic artery, the proximal aortic arch and the middle aortic arch. Maximal flow velocity (Vmax: m/sec) was measured by pulsed Doppler mode using transesophageal echogram (TEE) at the level of distal aortic arch, descending thoracic aorta of pulmonary trunk level and descending thoracic aorta at 10cm distal from the pulmonary trunk level. Measurement of flow pattern and velocity was done by an anesthetist who was blinded for results obtained in vitro study. Duplex scan and color image flow mapping was used to evaluate flow velocity and turbulence. Intraoperative duplex scan was recorded in videotape and reviewed by anesthetist. Data was expressed by mean ± SD. This study was approved by ethical committee in Hirosaki University School of Medicine.

Results

In the right axillary artery perfusion, Vmax in the proximal aortic arch near the ostium of the BCA reached 2.19 m/sec and the accelerated flow hit the lesser curvature of the aortic arch. Vmax in each level of the aorta is shown in the Figure 39. The turbulent flow was observed around the proximal aortic arch and the ascending aorta. By contrast, the flow became steady in the descending aorta. No patient exhibited stroke after surgery. Because flow velocity from the BCA in these patients was unexpectedly high and we experienced intraoperative aortic dissection due to the right axillary artery perfusion with cannulation, we changed our strategy from axillary artery perfusion as a single access to the aorta to combined perfusion from the axillary artery and the femoral artery for patients with small constitution. Therefore, in vivo study was completed in these three patients.

Perfusion from the right axillary artery
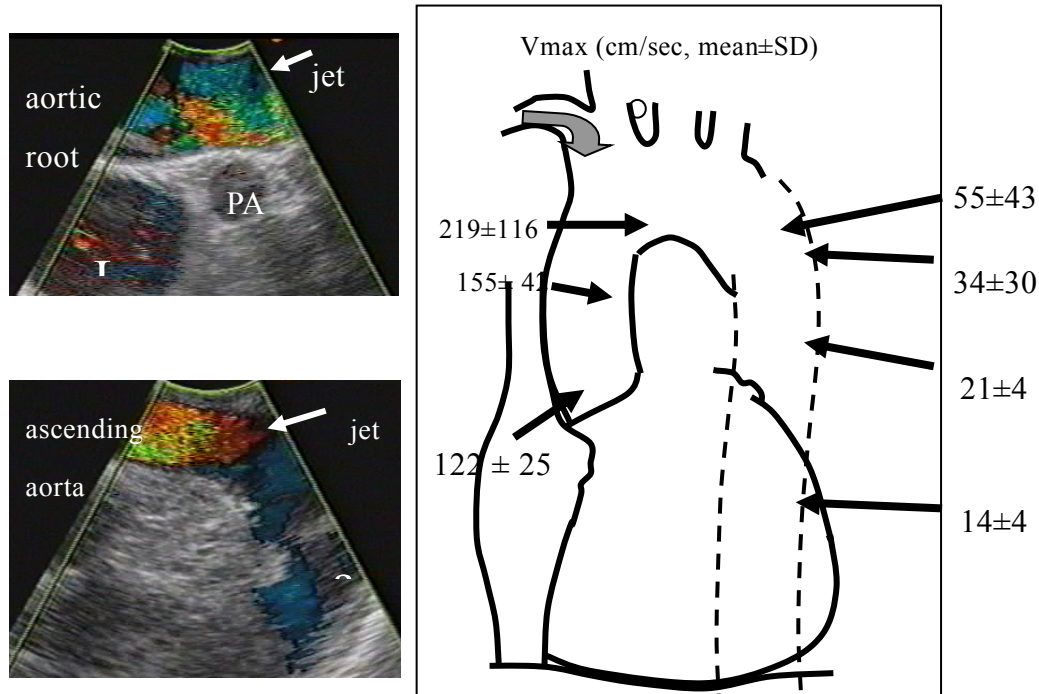
Fig 39. Perfusion from the right axillary artery

Discussion

In this clinical observation, we found accelerated flow velocity in the aortic arch in case of the left axillary perfusion with side-armed branch. Fast jet flow blows from the ostium of the BCA directing toward the lesser curvature of the aortic arch. Fast flow goes into the ascending aorta with mosaic pattern. Cardiovascular surgeon must bear in mind for this characteristic pattern of the left axillary artery perfusion when they perform operation using ECC upon patients with atherosclerotic degeneration of the aortic arch.

Chapter 4. Computed simulation of the aortic perfusion

Computer simulation of jet flow from the cannula was performed in normal and transverse aortic arch aneurysm model with an end-hole cannula and compared to the glass model experiment.

Methods

This study deals with the flow of an incompressible viscous fluid with constant properties. The continuity and Navier–Stokes equations for three-dimensional unsteady flow are written as follows:

$$\frac{Du}{Dt} = Fx - \frac{1}{\rho}\frac{\partial p}{\partial x} + \frac{\mu}{\rho}(\frac{\partial^2 u}{\partial x^2} + \frac{\partial^2 u}{\partial y^2} + \frac{\partial^2 u}{\partial z^2})$$

$$\frac{Dv}{Dt} = Fy - \frac{1}{\rho}\frac{\partial p}{\partial y} + \frac{\mu}{\rho}(\frac{\partial^2 v}{\partial x^2} + \frac{\partial^2 v}{\partial y^2} + \frac{\partial^2 v}{\partial z^2})$$

$$\frac{Dw}{Dt} = Fz - \frac{1}{\rho}\frac{\partial p}{\partial z} + \frac{\mu}{\rho}(\frac{\partial^2 w}{\partial x^2} + \frac{\partial^2 w}{\partial y^2} + \frac{\partial^2 w}{\partial z^2})$$

$$\frac{\partial u}{\partial x} + \frac{\partial v}{\partial y} + \frac{\partial w}{\partial z} = 0$$

where t denotes the time, u, v, w the velocity component for x, y, z axis, p the pressure, ρ the density, and μ the viscosity. To perform numerical simulation, 359809 cells were constructed in the virtual aortic model using trimmed cell meshing technique in STAR-CD (CD-adapco Japan Co. Ltd, Yokohama, Japan). Analysis for steady flow was carried out by inputting initial flow condition. To recreate flow vectors from cannula tip, virtual curved endhole cannula was reconstructed in the workstation using PRO-MODELER software (CD-adapco Japan), according to measured data of real endhole aortic cannula (Fig 40). Reconstructed cannula and virtual aortic model were captured into the 3-Matic software (Materialise Japan Co. Ltd. Yokohama, Japan) individually. Then each three-dimensional models were combined in virtual working space. The virtual cannula exit was subtracted from the virtual aortic model using Boolean operation. The position and direction of the virtual cannula were adjusted to simulate that of experimental glass model to

compare the data from the experimental model.

To calculate velocity distribution at the tip of endhole cannula, mathematical modeling of the curved endhole cannula was performed using pro STAR/amm. 304356 meshed cells were made in the virtual cannula. Initial flow velocity of 2.359m/s was given to the inlet of virtual cannula with transactional area of $2.8274 \times 10^{-5} m^2$. Flow volume in the cardiopulmonary bypass was set at 4.0 l/min. No slip condition was given at the wall of cannula. The flow at the outlet of cannula was set to flow out into virtual volume space in order to reduce the influence of outlet boundary condition. Water was used as perfusate to compare the real model experiment. Reynolds number was calculated by following equation.

$Re = (UD)/v$

where U is flow velocity at cannula inlet, D is diameter at cannula inlet ($6.0 \times 10^{-3} m$) and v is kinematic viscosity of fluid (water, 0.890 Pas). Since calculated Re was 15850, high Reynolds number k-ε model in STAR-CD was employed for flow simulation in endhole cannula. SIMPLE method was used to simulate steady flow in endhole cannula. Velocity contour of curved endhole cannula tip and distribution of velocity vector was shown in Fig3.

Calculated initial condition of flow at the cannula exit was given into the subtracted phantom of cannula tip in the virtual aortic model. SIMPISO method, combination of SIMPLE method and PISO method, was used as analytical algorism of flow analysis. SIMPISO method was advantageous to analyze flow in complicated three-dimensional configuration of this aortic aneurysm model. Low Reynolds number k-ε model was used for the simulation of the aortic model because the global flow velocity in the aortic model was slow. The boundary condition of the drainage of the aortic model was given as follows; the brachiocephalic artery 12.5%, the left common carotid artery 6.25%, the left subclavian artery 6.25% and the descending thoracic aorta 75% of flow with no slip condition. Shear stress was calculated using computing program in STAR-CD software and distribution of shear stress was depicted in three-dimensional map. Wall shear stress was calculated the following equation and depicted in the contour map of the aorta.

$$\text{Wall Shear Stress[Pa]} = \mu_{eff} \times \left(\frac{du}{dx}\right)$$

where µeff is sum of molecular viscosity and turbulence viscosity, du/dx is continuous velocity gradient in nearest-wall cell.

¶ 1. SIMPLE method: abbreviation of Semi-Implicit Method for Pressure-Linked Equation.¶2. PISO method: abbreviation of Pressure-Implicit with Splitting of Operators method

Results

1) Computed simulation of the aortic perfusion

Similar pattern of flow was observed in the ascending aorta and the transverse aorta in glass model experiment and computational simulation model in normal and aortic arch aneurysm model. Figure 6 shows flow velocity and flow vector in glass model and computational model. Flow velocity distribution was similar in two models. Similar vertical flow was generated in two models.
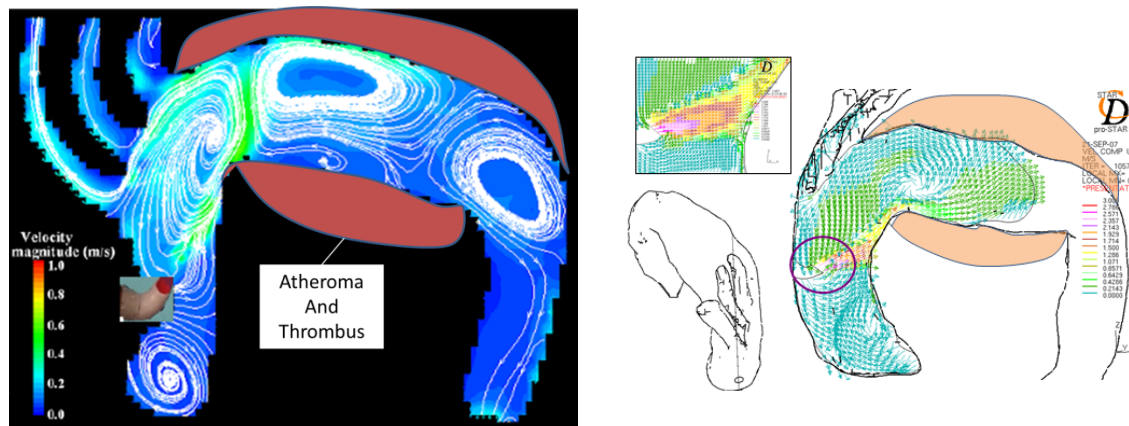
Figure 40. Flow map of jet from end-hole cannula in transverse aortic arch aneurysm model. Left; glass model. Right; computational model

Discussion

Atheroembolism after cardiac and thoracic vascular operation is emerging problem (Doty et al. 2003). In surgery of the transverse aortic arch aneurysm,

atheromatous change of the intima is severe and stroke is the most important problem. Perfusion strategy is very important to overcome atheroembolism in patients having severe atherosclerotic aorta. Several types of aortic perfusion cannula were developed to reduce sandblast effect to soft atheroma in the aorta. However, experimental technique to evaluate flow pattern and shear stress is not mature. Straight tubes were frequently used to evaluate flow as the mock aorta (White et al. 2009). Although it is simple method to evaluate competence of the cannula, it is not realistic model. Our approach is unique and realistic to evaluate flow velocity and shear stress in various shapes of the aorta. Computational model may be useful to evaluate flow in each patient in near future.

Conclusions

Computational flow simulation may be useful tool to determine cannulation site and type of cannula to decrease atheroembolic complication.

Section 2. Computed simulation of the femoral perfusion

The femoral artery has been one of the preferred arterial access sites for extracorporeal circulation because it is easy to expose and thick enough to insert the cannula (Lillehei and Cardozo, 1959). In the early days of extracorporeal circulation, the femoral artery was as popular as the aortic cannulation. However, aortic perfusion became dominant owing to improvement of cannula shape and secure cannulation techniques (Dewall and Levy, 1963). After advent of minimally invasive cardiac operation, femoral artery perfusion regained popularity (Navia et al. 1996) (Saunders et al., 2004). Aortic cannulation is less advantageous and sometimes risky through small thoracotomy. Femoral artery perfusion is also efficacious for cardiac reoperation or surgery of thoracic aorta. Although small perfusion cannula is advantageous in the context of minimally invasive surgery, femoral artery perfusion has several problems; 1) concern for cerebral embolism due to retrograde perfusion (Grossi et al., 2011; Chan et al., 2012; Murzi et al., 2013), 2) stress on the arterial wall and risk of arterial wall injury (Jones et al., 1960; Tanemoto et al., 1994), 3) malperfusion to the distal femoral artery (Palmer and Mercer, 1973).

Another approach of peripheral artery perfusion is axillar artery perfusion. It is well documented clinically and basically (Baribeau, 1998; Minakawa, 2008). Side-armed perfusion anastomosing prosthetic graft from the axillary artery is better than direct cannulation of the axillary artery (Svensson, 2004). Because the jet from the brachiocephalic artery may hit the lessor curvature, atheroembolism from the atherosclerotic aorta is not avoidable. We routinely employ side-armed perfusion not only from the axillar artery but also from the femoral artery.

The flow structures caused by the jet issued from the direct cannulation or the side-armed procedure are substantially different. Direct cannulation comprises parallel flow to the iliac artery. On the contrary, perfusion from side-armed graft comprises vertical flow to the vessel wall. The great advantage of side-armed graft perfusion seems to be its large caliber for the small sized femoral artery. But flow pattern from the femoral artery is not studied yet. The difference in inlets may result in crucial change in flow pattern, and thus in the occurrence of complications, in

femoral perfusion especially in the vicinity of the inlets because the diameter of the inlets are almost the same as ones of the vessels.

The characteristics of blood flow in extracorporeal circulation have been widely studied with the aid of computational fluid mechanics. However the main target of numerical simulation was the blood flow in aortic arch (Benim et al., 2011; Morris et al., 2005; Shahcheraghi et al., 2002; Tokuda et al., 2008) and a few study focused on the retrograde perfusion from femoral artery. Benim et al. (2011) simulated and compared the blood flow in physiological circulation, anterograde perfusion and retrograde perfusion. They concluded that with retrograde perfusion much higher wall shear stress could be caused in the femoral artery. In their simulation, however, only a cannula of specific diameter was inserted always perpendicular to the right femoral artery. The effect of several parameters, on femoral perfusion, such as the orientation of cannula and the ratio of diameters of cannula to vessel are yet to be revealed.

This study aims to clarify flow structures caused by a cannula or a graft with the aid of computational fluid dynamics.

Methods

Aortic modeling

A virtual blood vessel model from the ascending aorta to the femoral arteries was reconstructed from computed tomography images of a healthy adult man (age: 31 years, height: 177 cm, weight: 63 kg) (Fig. 41). Simulated flow analysis from the femoral artery was performed in this model. In the numerical simulations, incompressible Navier-Stokes equation and continuity equation were solved using commercial computed flow dynamics software (STAR-CD, CD-Adapco Japan Co. Ltd, Yokohama, Japan). The blood was assumed as a Newtonian fluid having the same dynamic viscosity and density of blood; $\mu = 3.8 \times 10^{-3}$ Pa·s, $\rho = 1050$ kg/m^3. Numerical meshes were constructed in the aortic model with 650,000 hexahedrons. Vessel walls were assumed to be rigid boundary with the no-slip condition. Steady flow calculation with convergent residual of 10^{-5} was conducted.

Condition of computed flow simulation

Uniform flow condition with constant flow rate of 4.248l/min (2.4L/m² for body surface area) was applied for the inlet boundary condition of numerical calculation. Initially simulated antegrade perfusion from the aortic orifice was calculated. Then retrograde perfusion from the femoral artery was simulated. The inlet flow was introduced through either a cannula or a graft from the right femoral artery. In the femoral artery cannulation model, the cannula was attached parallel to the right femoral artery. In the side-armed perfusion model, virtual graft was connected vertical to the right femoral artery (Fig. 42). The inner diameter of cannulas was set in two different sizes; 4 and 5.2 mm. The diameter of graft was set as 8 mm.

As the outlet boundary conditions, a porous media of calibrated resistance was connected on the outlet of each vessel branch in order to simulate capillary vessels following the data by Yull Park et al. (2007). The diameter of the porous media was 10 or 15 mm, and the length was 30 mm. The pressure at the outlet of the porous media was set at venous pressure, 1.3 kPa. The flow rate through each porous media depends on resistance coefficient which was given for each branch in the literature in the case of normal anterograde circulation. The same resistance coefficient was used for numerical simulation in femoral perfusion model.

Evaluation of flow simulation

In addition to the numerical simulation of blood flow from the aortic orifice (normal) model, we conducted numerical experiments on the cannula perfusion from a femoral artery. In this simulation, the jet issued from a cannula to the femoral artery was simulated by a pipe flow with a sudden expansion. Six different conditions on the combination of the diameters of cannula and vessel were examined; cannula diameter for 4 or 5.2 mm, vessel diameter for 7, 10 or 15 mm. The inlet and outlet boundary conditions were given by constant flow rate of 4.248l/min in all these numerical experiments. Other conditions including physical properties of test fluid and wall boundary conditions were same as ones for the simulation with normal model shown above.

Distribution of flow volume, distribution of flow velocity in the iliac artery and

shear stress to the iliac artery were calculated in the CFD software.

Results

1. Difference in flow characteristics between anterograde and retrograde vascular flow

Change of the flow volume into each vessel branch between physiological anterograde perfusion and artificial retrograde vascular flow were compared. The base line simulation was carried out in the inlet at the aortic ostium with the porous media at all the outlets including the right femoral artery. For the simulation of retrograde circulation from the femoral artery, the perfusion with both the cannula and graft were introduced from the femoral artery.   Flow volume distribution at each branch under the physiological antegrade condition (normal) and the retrograde perfusion with cannulas and graft are shown in Table 3. The deviations in flow volume from the physiological condition in retrograde perfusion are also depicted. It is found that with the cannula the flow rates through all the outlets except for the right internal iliac artery increase by 5 to 7 %. This increase in flow rates was caused by the blockage of blood flow distal to the right femoral artery due to insertion of the cannula. On the other hand, with graft, the blood flow rate as well as pressure in the distal region increases by 50 %, which results in the decrease in blood flow to other branches by 1 to 5 % (Table 4).

The largest decrease in flow rate was found in right internal iliac artery in both the cannula and the graft perfusion model. To investigate the reason for this decrease, we next focus on the change in flow pattern near the bifurcation of the common right iliac artery. Figure 43 shows the velocity vectors on the sagittal plane including the axis of the iliac bifurcation for the physiological flow and the retrograde flow with cannula. It clearly shows perfusion with cannula makes several times faster flow than that with physiological condition.   In the antegrade perfusion the vascular flow diverse almost evenly into each branch at the iliac bifurcation, whereas in the retrograde perfusion the fast flow from femoral artery was not able to bend the corner due to the large inertia. The fast stream separates and causes a

recirculation region at the corner. This recirculation resulted in the decrease in flow rate to the right internal iliac even with relatively large average flow rate at the junction.

2. Difference in flow characteristics between cannula and graft perfusions

In this section, focus is paid on the difference in flow pattern and the corresponding wall shear stress cause by the jet issued from the cannula or the graft. In Fig. 44, the contours of shear stress on the vessel wall in the vicinity of the inlets are shown. The overall shear stress decreases in the graft perfusion model in comparison to the cannula perfusion model. It is simply because divergence of flow was observed at inlets in the graft perfusion and less flow volume issued into the right femoral artery in cannula perfusion model. Quantitatively, the highest shear stress of 172 Pa was observed with the small-diameter cannula (4mm in diameter) among the three conditions, following 127 Pa with the graft (8 mm in diameter) and 99 Pa with the large-diameter cannula (5.2 mm in diameter).

The lowest shear stress was observed in 5.2mm cannula perfusion even though the jet velocity at the exit of cannula was faster than that of the graft (Fig. 44). While the maximum shear stress areas appeared on the external iliac artery in the cannula perfusion model, it appeared on the common femoral artery in the graft perfusion model. Distribution of the velocity vectors are depicted in Fig. 45. It is clearly shown that the relaxation distance for the jet to impinge to the vessel wall was about 2.5 times longer with the cannula than the graft because of difference in the way of connection; parallel or vertical to the vessel.

3 Relaxation distance for the development of the jet from the cannula in femoral artery

As the maximum shear stress area appears at the impingement point of the jet from the cannula, relationship between diameter of the femoral artery and the cannula should be evaluated. It is because the relaxation distance before the impingement to the vessel wall is required for the jet flow to create maximum shear stress area. To explore this relationship, numerical examination of the difference in jet profiles in pipe flow with sudden expansion was performed. The six conditions

with different diameters of cannula and vessels as denoted in the previous chapter were tested.

The variation of maximum axial speed at the jet center along the co-axis of the pipe is shown in Fig. 46 (a). The origin of horizontal axis corresponds to the sudden expansion. Characteristic of the jet behind a sudden expansion is shown in this figure; the jet speed decreases due to the Coanda effect caused by the recirculation behind the sudden expansion and keeps a constant speed after the reattachment length of the flow. The reattachment length is found to be strongly depends on the vessel diameter R_2 as indicated by the result that each two lines of the same color reach a constant velocity at almost the same distance.

In Fig. 46 (b), we re-plot the same data as in (a) but in dimensionless form. The velocity is standardized by percentage, so that it changes in the range between 1 and 0 corresponding to maximum and minimum velocity respectively. The distance from the sudden expansion was normalized by a length scale $(R_2 - R_1)/\ln(R_2/R_1)$ which is a measure for the radius of curvature in the recirculation zone behind the sudden expansion (Vanierschot and Van den Bulck, 2008). It is shown that all the data collapses into a single curve with this normalization. This study revealed that the normalized distance converges around length scale 6 for the variations in both cannula and vessel diameters in the femoral artery perfusion model.

Discussion

The femoral artery is regaining popularity as the arterial access in minimally invasive cardiac surgery recently. It is one of the thickest arteries existing near the surface of the human body. Therefore, it is easy to expose with small incision comparing to the axillary artery. It is advantageous in the context for minimally invasive cardiac surgery. Average diameter of the femoral artery is 8 to 10 mm in adult. Despite its easiness to exposure, there are several disadvantages in femoral artery perfusion; reverse atheroembolism, intimal injury and ischemia of the ipsilateral leg.

1. Reverse atheroembolism

The major concern of the femoral artery perfusion is "reverse" atheroembolism because flow from the femoral artery to visceral arteries and cerebral arteries is retrograde fashion. In aged patients, atherosclerosis creates soft plaques protruding into the lumen of the descending aorta, the abdominal aorta and the iliac artery. Detachment of this flail atheroma will cause atheroembolism to visceral organs and the brain. When small pieces of atheroma occlude endartery of the lower extremities, it is called blue toe syndrome. The most frequent embolic source of blue toe syndrome is the abdominal aorta or the iliac artery (O'Keeffe et al., 1992). As shown in this study, retrograde perfusion generates fast velocity flow in the external and common iliac artery. When the fast jet flow impinges on the atheromatous iliac artery, flail plaque may detach causing embolism to the visceral organs or brain. Price et al. reported cholesterol embolism caused by retrograde femoral artery perfusion in cardiac surgery (Price and Harris, 1970). Study in cardiac reoperation revealed the femoral artery perfusion was the significant risk factor for cerebral complication in multivariate analysis (Crooke et al. 2010). On the contrary, Yale University group investigated complications of femoral artery perfusion in 880 patients undergoing thoracic aortic surgery and reported a 1.8% incidence of permanent stroke. They evaluated the descending thoracic aorta using transesophageal echogram, and the cannulation site was changed to the axillary artery when mobile atheroma was detected (Ayyash et al., 2011). Our study showed information regarding this issue. 1) Small-size cannula generates swift jet flow in the external and common iliac artery generating extremely high shear stress area. This data suggests cannula with large diameter is better than small diameter cannula. 2) Although perfusion from the graft generates higher shear stress area at the junction of the femoral artery and the graft, flow velocity profile in the ipsilateral iliac arteries was generally slow. In clinical practice, anastomosis of the graft to the femoral artery is performed only on healthy artery free of atherosclerosis. 3) Velocity profile changes according to size of the femoral artery, size of cannula, position of the cannula tip and configuration of the iliac artery. Result of this study showed distance-flow velocity curve comprises sigmoid curve and wider the arterial diameter, steeper the decrease of flow velocity.

In clinical practice, cannula tip is placed deep into the external iliac artery. This relationship should be analyzed in the future.

2. Mechanical injury due to the femoral artery perfusion

One of the serious complications in the femoral artery perfusion is injury to the femoral and the iliac artery, such as aortic dissection. As shown in our study, high shear stress appeared in the femoral perfusion with small-sized cannula. Because high shear stress area corresponds to impingement point of flow to the vessel wall, care must be taken not to insert small-sized cannula deep into the external iliac artery.

3. Malperfusion to the distal femoral artery

The most tragic complication of the femoral artery cannulation is acute limb ischemia due to malperfusion to the distal femoral artery (Palmer and Mercer, 1973; Hendrickson and Glower, 1998). In femoral artery cannulation, distal stamp of the arteriotomy is clamped. It will induce ischemia of the limb. Within 3 hours of warm ischemia, muscle function is maintained and reversible. In experimental study, capillary permeability is maintained even after 4 hours of warm ischemia. However, ischemia-reperfusion injury may occur for longer period of ischemia. Anastomosing graft to the femoral artery is one of solution for this complication.

Conclusions

The femoral artery perfusion with three different types was investigated numerically. Small-sized cannula generates extremely high shear stress area on the external iliac artery. Velocity magnitude of cannula exit is high even if 5.2 mm cannula is used. Side-armed perfusion with 8mm graft may attenuate generation of high shear stress area on the external iliac artery.

perfusion and direct femoral artery perfusion. Kitamura S, Shirota M, Fukuda W, Inamura T, Fukuda I. J Artif Organs. 2016 Dec;19(4):336-342.

	normal	cannula		graft	
	(L/min)	(L/min)	difference (%)	(L/min)	difference (%)
Brachiocephalic	0.510	0.533	4.6	0.478	-6.2
Left common carotid	0.278	0.293	5.4	0.264	-4.8
Left subclavian	0.232	0.242	4.3	0.228	-1.6
Celiac	0.680	0.758	11.6	0.686	1.0
Superior mesenteric	0.510	0.539	5.8	0.496	-2.6
Right renal	0.510	0.553	8.4	0.494	-3.1
Left renal	0.510	0.552	8.2	0.495	-2.9
Right common liliac	0.255	0.249	-2.1	0.233	-8.7
Left common liliac	0.255	0.265	3.8	0.244	-4.3
Right femoral	0.153	0.000		0.233	52.2
Left femoral	0.153	0.159	4.1	0.145	-5.0
Right circumflex	0.102	0.000		0.155	52.3
Left circumflex	0.102	0.105	3.0	0.096	-5.7
Total	4.248	4.248	0	4.248	0

Table 3. Comparison in flow rate into each branch with cannula or graft

Table 4 Comparison of flow volume in each method

	normal (L/min)	cannula (L/min)	difference (%)	graft (L/min)	difference (%)
BCA	0.510	0.533	4.6	0.478	-6.2
Left common carotid	0.278	0.293	5.4	0.264	-4.8
LSCA	0.232	0.242	4.3	0.228	-1.6
Celiac	0.680	0.758	11.6	0.686	1.0
Superior mesenteric	0.510	0.539	5.8	0.496	-2.6
Right renal	0.510	0.553	8.4	0.494	-3.1
Left renal	0.510	0.552	8.2	0.495	-2.9
Right internal iliac	0.255	0.249	-2.1	0.233	-8.7
Left internal iliac	0.255	0.265	3.8	0.244	-4.3
Right superficial femoral	0.153	0.000		0.233	52.2
Left superficial femoral	0.153	0.159	4.1	0.145	-5.0
Right deep femoral	0.102	0.000		0.155	52.3
Left deep femoral	0.102	0.105	3.0	0.096	-5.7
Total	4.248	4.248	0	4.248	0

Fig. 41. Aortic model reconstructed from a series of CT images

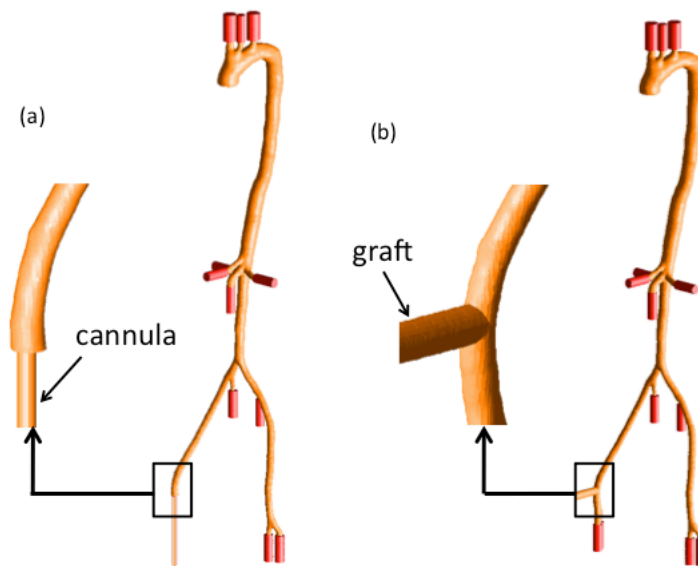Fig 42. Numerical simulation model with (a) cannula and (b) graft as an inlet. Small cylinders on each branch indicates simulated capillaries.
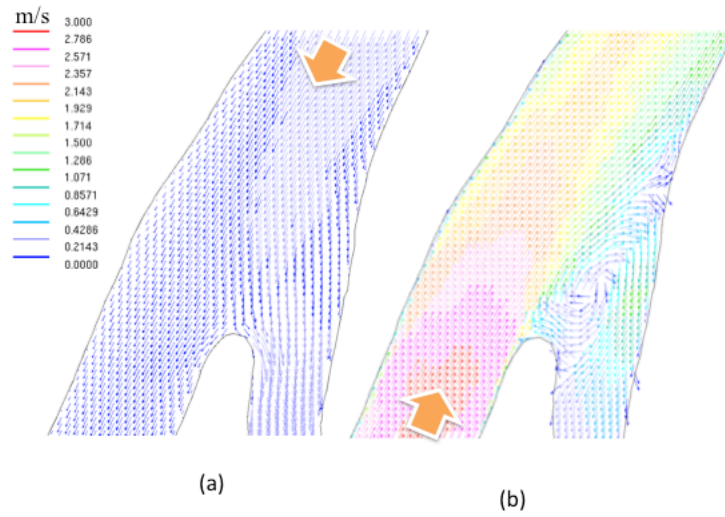
Fig. 43 Velocity vectors in the bifurcation of the common right iliac artery.
(a) physiological flow and (b) retrograde perfusion with cannula.
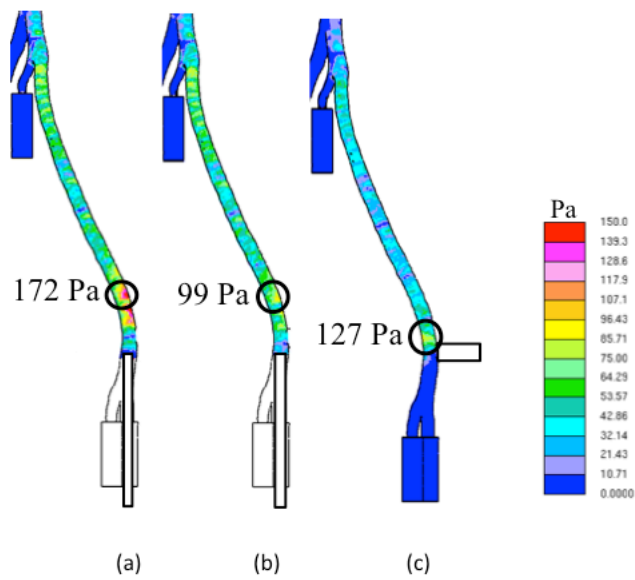
Fig. 44 Wall shear stress distribution near the inlet with a (a) cannula of 4 mm,
(b) cannula of 5.2 mm and (c) graft of 8 mm.

Fig. 45 Velocity vectors near the inlet with a (a) cannula of 4 mm, (b) cannula of 5.2 mm and (c) graft of 8 mm. The region where the highest shear stress was observed was marked with red circle for each case.

Fig. 46 Variation in maximum axial velocity after the sudden expansion. (a) original and (b) normalized data.

Chapter 5 Clinical application and Future of flowdynamics in cardiovascular surgery

Section 1. Development of Atherosclerotic Model Specific for Humans
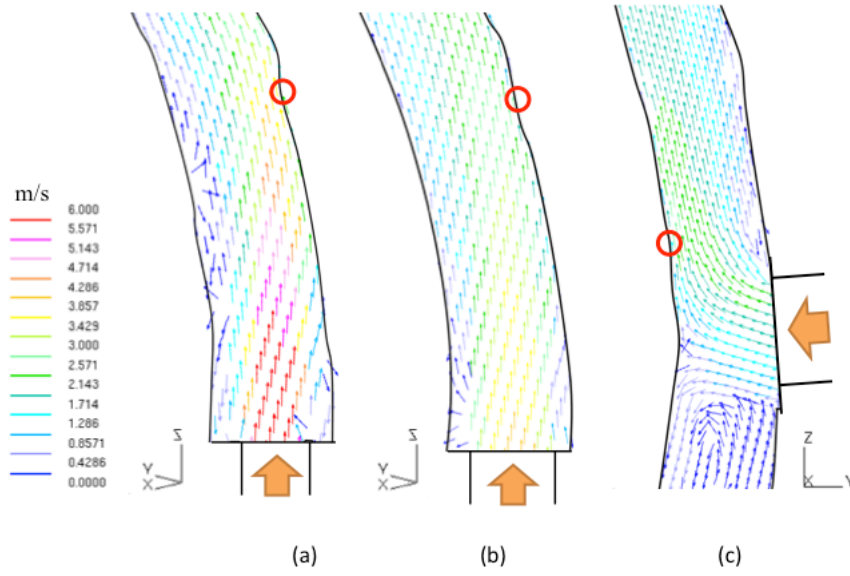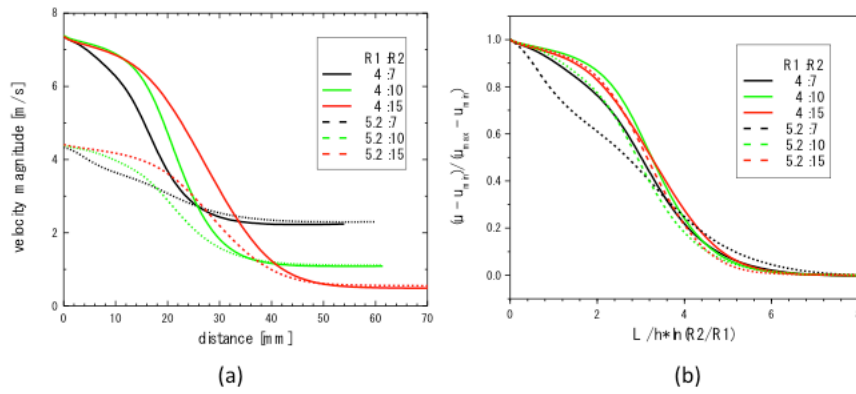
Etiology of atherosclerosis had been long-standing controversy in the 20th century. Dyslipidemia was not always accepted as a significant factor in atherosclerosis and coronary heart disease in the previous century (Steinberg, D. J. Lipid Res. 2004). In 1913, Nikolai Anitschkow, a Russian pathologist developed a rabbit model of atherosclerotic disease by feeding lipid-rich diet. Some laboratories tried to confirm his findings, but instead of using rabbits, most of them used rats or dogs because these experimental animals were familiar with their laboratories. Cholesterol feeding in these species failed to induce atherosclerotic lesions. As a result, his findings were largely rejected. Cholesterol theory had not been widely accepted until the mid-twentieth century. Experimental model of atherosclerosis in large animal is difficult. Cost of breeding the large animal is expensive and it takes long time to be old enough to have atherosclerotic diseases. Morphology of the aorta in swine or sheep is different from the human aortic system. In swine, the ascending aorta is short. The aortic arch vessels are two branches rather than three branches in humans; the brachiocephalic artery branching the right subclavian artery plus bilateral carotid arteries and the left subclavian artery. Therefore, it is very difficult to reproduce animal aortic arch model to simulate atherosclerotic aorta of humans.

Another problem is a choice of appropriate method for flow measurement. One of flow measurement methods is duplex scan. Advantage of the duplex scan is real time measurement of flow during experimental study or surgery. Flow map can be shown by color doppler scan. Velocity can be measured by pulse doppler method in vivo. Although intraoperative measurement of flow on arterial perfusion cannula is real time study, it disrupts surgical procedure during operation. Comparison of flow in the same patient is not justified ethically. Trans-esophageal ultrasonography is another option. However, the aortic arch sometimes become

blind spot due to air in the trachea and the bronchus.

Cardiac magnetic resonance imaging (cine MRI) enables high-resolution assessment of aortic flow and geometry. It is useful method for evaluation of in vivo flow and is especially useful to analyze intra-aortic blood flow in various pathology such as aortic aneurysm, aortic dissection and aortopathy in bicuspid aortic valve under physiological condition. Blood flow is expressed as flow vectors in cine MRI. It is also useful to evaluate four-dimensional aortic flow after reconstruction of the aorta (Gaudino M et al. J Thorac Cardiovasc Surg 2019). Analysis of flow streamline and wall shear stress are computed by specific program. Flow streamline can be expressed on arbitrary plane. Many studies observed flow in the aorta using MRI. However, real time MRI analysis is difficult for patients undergoing extracorporeal circulation. Background of patients undergoing surgery using extracorporeal circulation is diverse for a body size, morphology of the aorta, flow volume of the extracorporeal circulation and the degree of atherosclerotic change. Using our experimental system with PIV method, we can observe and compare flow functions of various cannulas under the fixed condition. Using this method, we can evaluate detailed characteristic of flow-traces in various cannulas and arterial routes.

Disadvantage of the glass model analysis is as follows; 1) the scale of the analytic instrument is large; 2) there are blind spots due to the shadow of cannula; 3) fine tuning of the equipment is necessary to obtain stable results; 4) it is difficult to make patient-specific glass models for each morphology. Development of an easier and case-specific transparent aortic model is required; however, as shown in Chapter 2, three-dimensional modelling using 3D printer is not satisfactory on the aspect of transparency, waterproof property and smoothness of the inner surface for the aortic model. To overcome these problems, computed flow-analysis is useful emerging technique. In the present study, we only applied simple cannula model such as perfusion from end-hole cannula of the aortic perfusion or side-armed perfusion from the peripheral arteries. To calculate perfusion from the dispersive cannulas, data for initial condition of flow velocity and vectors is

necessary. To recreate more realistic models, further study on clinical models comparing with computed analysis is necessary.

Section 2. Clinical relevance

Our experimental study on aortic perfusion directing Dispersion cannula toward aortic root gave important impact on the management of aortic arch replacement with significant atherosclerosis on the aortic arch. Okita and Okada et al. (Okada K, et al. J Thorac Cardiovasc Surg. 2013) (Okita Y et al. J Thorac Cardiovasc Surg. 2013;)(Okita Y. Ann Cardiothorac Surg. 2018) reported efficacy of cannula tip directing toward aortic root in surgery for severe atherosclerotic aortic arch. They referred our results as follows. "24F dispersion cannulas were used more often in patients with an atherothrombotic aorta and were used in 85.3% of patients in this group. This was in accordance with the findings from Fukuda and associates, who demonstrated that directing the cannula tip of the dispersion cannula toward the aortic root generated slower and less turbulent flow in the transverse arch of the glass models of both healthy and aneurysmal aortic arches." They also referred our experimental study as disadvantage of the axillary artery perfusion in the atherosclerotic aortic arch as follows. "Right axillary artery perfusion is one of the useful options for arterial cannulation, and its efficacy has been reported. However, the perfusion has some problems with regard to the hydrodynamic properties. Minakawa and associates performed a streamline analysis of the right axillary artery perfusion in the aortic arch aneurysm model. The flow jet with rapid velocity strikes on the posterior wall of the ascending aorta and enters the ascending aorta with vortical flow that is unexpectedly rapid. This type of nonphysiologic flow causes the detachment of atheroma, with the debris consequently washed away into the left common carotid artery." Yamana et al. reported clinical evaluation of flow velocity using duplex scan during aortic arch surgery when cannula tip directed toward aortic root (Yamana K et al. Ann Thorac Surg. 2010). They observed the similar flow pattern in 15 patients undergoing aortic arch surgery.

We developed a new cannula generating more gentle flow to the aorta from series of our experiments; the "Stealthflow cannula". Flow velocity and shear stress were analyzed using PIV method (Goto T et al. Hydrodynamic evaluation of a new dispersive aortic cannula (Stealthflow). J Artif Organs. 2016). Clinical outcome of Stealthflow cannula is also excellent.

Our studies were unique and clinically important to clarify flowdynamics and atherosclerotic lesion on the inner surface of the aorta. This method is useful to resolve atheroembolic complications in aortic surgery and open-heart surgery using extracorporeal circulation. Development of computed simulation method for more complicated aortic morphology and cannula shape is required to apply flowdynamic study in surgical practice. Case specific approach using computer simulation method will be necessary for more reliable method in the future.

Chapter 6. Bibliography

Albert AA, Beller CJ, Arnrich B, Walter JA, Rosendahl UP, Hetzel A, Priss H, Ennker J. Is there any impact of the shape of aortic end-hole cannula on stroke occurrence? Clinical evaluation of straight and bent-tip aortic cannulae. Perfusion. 2002; 17: 451-456

Almassi GH1, Sommers T, Moritz TE, Shroyer AL, London MJ, Henderson WG, Sethi GK, Grover FL, Hammermeister KE. Stroke in cardiac surgical patients: Determinants and outcome. Ann Thorac Surg 1999; 68: 391-398

Ayyash B, Tranquilli M, Elefteriades JA. 2011 Femoral artery cannulation for thoracic aortic surgery: safe under transesophageal echocardiographic control. J Thorac Cardiovasc Surg. 142, 1478-81

Baribeau YR, Westbrook BM, Charlesworth DC, Maloney CT. 1998 Arterial inflow via an axillary artery graft for the severely atheromatous aorta. Ann Thorac Surg. 6, 33-7.

Benim, AC, Nahavandi, A, Assmann, A, Schubert, D, Feindt, P, Suh, SH. Simulation of blood flow in human aorta with emphasis on outlet boundary conditions. Appl Math Model 2011; 35: 3175– 3188.

Blauth CI, Cosgrove DM, Webb BW, Ratliff NB, Boylan M, Piedmonte MR, Lytle BW, Loop FD.. Atheroembolism from the ascending aorta. An emerging problem in cardiac surgery.   J Thorac Cardiovasc Surg. 1992; 103: 1104-1012

Calafiore AM, Di Mauro M, Teodori G, Di Giammarco G, Cirmeni S, Contini M, Iacò AL, Pano M. Impact of aortic manipulation on incidence of cerebrovascular accidents after surgical myocardial revascularization. Ann Thorac Surg. 2002;73:1387-93

Chan EY, Lumbao DM, Iribarne A, Easterwood R, Yang JY, Cheema FH, Smith CR, Argenziano M. Evolution of cannulation techniques for minimally invasive cardiac surgery: a 10-year journey. Innovations (Phila). J 2012;7:9-14.

Chandran KB. Flow dynamics in the human aorta. J Biomech Eng. 1993; 115:611-616

Crooke GA, Schwartz CF, Ribakove GH, Ursomanno P, Gogoladze G, Culliford AT, Galloway AC, Grossi EA. Retrograde arterial perfusion, not incision location, significantly increases the risk of stroke in reoperative mitral valve procedures. Ann Thorac Surg. 2010; 89:723-9

Dewall RA, Levy MJ. Direct cannulation of the ascending aorta for open-heart surgery. J Thorac Cardiovasc Surg. 1963;45:496-9.

Djaiani G, Fedorko L, Borger M, Mikulis D, Carroll J, Cheng D, Karkouti K, Beattie S, Karski J. Mild to moderate atheromatous disease of the thoracic aorta and new ischemic brain lesions after conventional coronary artery bypass graft surgery. Stroke. 2004;35:e356-8

Doty JR, Wilentz RE, Salazar JD, Hruban RH, Cameron DE. Atheroembolism in cardiac surgery. Ann Thorac Surg. 2003;75:1221-6.

Eagle KA, Guyuton RA, Davidoff R, Hillis LD, Edwards FH, Hutter AM et al. ACC/AHA 2004 Guideline update for coronary artery bypass graft surgery. www.acc.org. 2004; e341-438

Endo S, Sohara Y, Karino T. Flow patterns in dog aortic arch under a steady flow condition simulating mid-systole. Heart Vessels. 1996; 11: 180-191

Flege JB, Aberg T. Transventricular aortic cannulation for repair of aortic dissection. Ann Thorac Surg 2001: 72; 955–6.

Fukuda I, Aikawa S, Imazuru T, Osaka M. Transapical aortic cannulation for acute aortic dissection with diffuse atherosclerosis. J Thorac Cardiovasc Surg 2002; 123: 369–70.

Fukuda I, Minakawa M, Fukui K, Taniguchi S, Daitoku K, Suzuki Y, Hashimoto H. Breakdown of atheromatous plaque due to shear force from arterial perfusion cannula. Ann Thorac Surg. 2007;84:e17-8

Fukuda I, Yanaoka H. Cannulas for extracorporeal circulation. Kyobu Geka. 2009;62(8 Suppl):661-5.

Gaudino M, Piatti F, Lau C, Sturla F, Weinsaft JW, Weltert L, Votta E, Galea N, Chirichilli I, Di Franco A, Francone M, Catalano C, Redaelli A, Girardi LN, De Paulis R. Aortic flow after valve sparing root replacement with or without

neosinuses reconstruction. J Thorac Cardiovasc Surg 2019;157:455-65

Gerdes A, Joubert-Hubner E, Esders K, Sievers HH. Hydrodynamics of aortic arch vessels during perfusion through the right subclavian artery. Ann Thorac Surg. 2000;69:1425-30

Gold JP, Torres KE, Maldarelli W, Zhuravlev I, Condit D, Wasnick J. Improving outcomes in coronary surgery: the impact of echo-directed aortic cannulation and perioperative hemodynamic management in 500 patients. Ann Thorac Surg. 2004 ;78:1579-85.

Goto T, Inamura T, Shirota M, Fukuda W, Fukuda I, Daitoku K, Minakawa M, Ito K Hydrodynamic evaluation of a new dispersive aortic cannula (Stealthflow). J Artif Organs. 2016;19:121-7

Groom RC, Hill AG, Kuban B, Oneill W, Akl BF, Speir AM, Koningsberg J, SprisserGT, Shakoor M, Massimiano PS, Burton NA, Albus RA, Macmanus Q, Lefrak EA. Aortic cannula velocimetry. Perfusion. 1995; 10: 183-188

Grooters RK, Thieman KC, Schneider RF, Nelson MG. Assessment of perfusion toward the aortic valve using the new dispersion aortic cannula during coronary artery bypass surgery. Tex Heart Inst J. 2000;27:361-5.

Grooters RK, Ver Steeg DA, Stewart MJ, Thieman KC, Schneider RF. Echocardiografic comparison of the standard end-hole cannula, the soft-flow cannula, and the dispersion cannula during perfusion into the aortic arch. Ann Thorac Surg 2003; 75: 1919-23

Grossi EA, Loulmet DF, Schwartz CF, Solomon B, Dellis SL, Culliford AT, Zias E, Galloway AC. Minimally invasive valve surgery with antegrade perfusion strategy is not associated with increased neurologic complications. Ann Thorac Surg. 2011;92: 1346-9

Hendrickson SC, Glower DD. A method for perfusion of the leg during cardiopulmonary bypass via femoral cannulation. Ann Thorac Surg. 1998;65:1807-8.

Hosoda Y, Watanabe M, Hirooka Y, Ohse Y, Tanaka A, Watanabe T. Significance of atherosclerotic changes of the ascending aorta during coronary bypass surgery with intraoperative detection by echography. J Cardiovasc Surg. 1991; 32: 301-306.

Inamura T, Yanaoka H, Yamazaki J, Fukuda I, Minakawa M, Fukui K. Visualization of blood flow in aortic arch by using PIV method (In case of cannula insertion). Transactions of Japan Society of Mechanical Engineers, Series B 2005; 710: 2385-92

Jones TW, Vetto RR, Winterscheid LC, Dillard DH, Merendino KA. Arterial complications incident to cannulation in open-heart surgery with special reference to the femoral artery. Ann Surg. 1960; 152:969-74.

Joubert-Hubner E, Gerdes A, Klapproth P, Esders K, Prosch J, Henke P, Pfister G, Sievers HH. An in-vitro evaluation of aortic arch vessel perfusion characteristics comparing single versus multiple stream aortic cannulae. Eur J Cardiothorac Surg. 1999;15:359-64.

Joubert-Huebner E, Gerdes A, Sievers HH. An in vitro evaluation of a new cannula tip design compared with two clinically established cannula-tip designs regarding aortic arch vessel perfusion characteristics. Perfusion. 2000; 15: 69-76

Katz ES, Tunick PA, Rusinek H, Ribakove G, Spencer FC, Kronzon I. Protruding aortic atheromas predict stroke in elderly patients undergoing cardiopulmonary bypass: experience with intraoperative transesophageal echocardiography. J Am Coll Cardiol. 1992;20:70-7.

Kazui T, Yamashita K, Washiyama N, Terada H, Bashar AH, Suzuki K, Suzuki T. Aortic arch replacement using selective cerebral perfusion. Ann Thorac Surg 2007;83:S796–8

Kilner PJ, Yang GZ, Mohiaddin RH, Firmin DN, Longmore DB. Helical and retrograde secondary flow patterns in the aortic arch studied by three-directional magnetic resonance velocity mapping. Circulation 1993; 88[part 1]: 2235-47

Kokotsakit J1, Lazopoulos G, Milonakis M, Athanasiadis G, Romana K, Skouteli E, Bastounis E. Right axillary artery cannulation for surgical management of the hostile ascending aorta. Tex Heart Inst J. 2005;32:189-93

Kvitting JE, Ebbers T, Wigstrom L, Olin CL, Bolger AF. Flow patterns in the aortic root and the aorta studied with time-resolved, 3-dimentional, phase-contrast magnetic resonance imaging: Implications for aortic valve-sparing surgery. J Thorac

Cardiovasc Surg 2004;127: 1602-7

Lillehei CW, Cardozo RH. Use of median sternotomy with femoral artery cannulation in open cardiac surgery. 1959 Surg Gynecol Obstet. 108,706-14

McKhann GM, Goldsborough MA, Borowicz LM Jr, Mellits ED, Brookmeyer R, Quaskey SA, Baumgartner WA, Cameron DE, Stuart RS, Gardner TJ. Predictors of stroke risk in coronary artery bypass patients.   Ann Thorac Surg. 1997; 63: 516-521

Mills NL, Everson CT. Atherosclerosis of the ascending aorta and coronary artery bypass. Pathology, clinical correlates, and operative management. J Thorac Cardiovasc Surg. 1991; 102: 546-553.

Minakawa M, Fukuda I, Inamura T, Yanaoka H, Fukui K, Daitoku K, Suzuki Y, Hashimoto H. Hydrodynamic evaluation of axillary artery perfusion for normal and diseased aorta.   Gen Thorac Cardiovasc Surg. 2008;56:215-21

Mori D, Yamaguchi T. Computational fluid dynamics modeling and analysis of the effect of 3-D distortion of the human aortic arch. Comput Methods Biomech Biomed Engin. 2002; 5: 249-260.

Morris L1, Delassus P, Callanan A, Walsh M, Wallis F, Grace P, McGloughlin T.3-D numerical simulation of blood flow through models of the human aorta. J Biomech Eng. 2005 ;127:767-75

Muehrcke DD, Cornhill JF, Thomas JD, Cosgrove DM. Flow characteristics of aortic cannulae J Card Surg. 1995; 10: 514-519

Murzi M, Cerillo AG, Miceli A, Bevilacqua S, Kallushi E, Farneti P, Solinas M, Glauber M. Antegrade and retrograde arterial perfusion strategy in minimally invasive mitral-valve surgery: a propensity score analysis on 1280 patients. Eur J Cardiothorac Surg. 2013;43:e167-72.

Navia JL, Cosgrove DM 3rd. Minimally invasive mitral valve operations. Ann Thorac Surg. 1996;62:1542-4.

Numata S, Ogino H, Sasaki H, et al. Total arch replacement using antegrade selective cerebral perfusion with right axillary artery perfusion. Eur J Cardiothorac Surg 2003;23:771–5

O'Keeffe ST, Woods BO, Breslin DJ, Tsapatsaris NP. Blue toe syndrome. Causes

and management. Arch Intern Med. 1992;152:2197-202.

Okada K, Omura A, Kano H, Inoue T, Oka T, Minami H, Okita Y. Effect of atherothrombotic aorta on outcomes of total aortic arch replacement. J Thorac Cardiovasc Surg. 2013;145(4):984-991.

Okano M, Yoshida Y. Influence of shear stress on endothelial cell shapes and junction complexes at flow dividers of aortic bifurcations in cholesterol-fed rabbits. Frontiers Med Biol Engng 1993; 5: 95-120

Okita Y, Minatoya K, Tagusari O, Ando M, Nagatsuka K, Kitamura S. Prospective comparative study of brain protection in total aortic arch replacement: deep hypothermic circulatory arrest with retrograde cerebral perfusion or selective ante-grade cerebral perfusion. Ann Thorac Surg 2001;72:72–9

Okita Y, Okada K, Omura A, Kano H, Minami H, Inoue T, Miyahara S. Total arch replacement using antegrade cerebral perfusion. J Thorac Cardiovasc Surg. 2013;145(3 Suppl):S63-71.

Okita Y. Neuro-protection in open arch surgery. Ann Cardiothorac Surg. 2018;7:389-396

Palmer BV, Mercer JL. Anterior tibial compartment syndrome following femoral artery perfusion. Thorax. 1973;28:492-4.

Price DL, Harris J. Cholesterol emboli in cerebral arteries as a complication of retrograde aortic perfusion during cardiac surgery. Neurology 1970;20:1209-14.

Rao V, Christakis GT, Weisel RD, Ivanov J, Peniston CM, Ikonomidis JS, Shirai T. Risk factors for stroke following coronary bypass surgery. J Card Surg 1995; 10: 468-74.

Ribakove GH1, Katz ES, Galloway AC, Grossi EA, Esposito RA, Baumann FG, Kronzon I, Spencer FC. Surgical implications of transesophageal echocardiography to grade the atheromatous aortic arch. Ann Thorac Surg. 1992;53:758-61

Sabik JF, Lytle BW, MaCarthy PM, Cosgrove DM. Axillary artery: an alternative site of arterial cannulation for patients with extensive aortic and peripheral vascular disease. J Thorac Cardiovasc Surg 1995;109:885-90

Saunders PC, Grossi EA, Sharony R, Schwartz CF, Ribakove GH, Culliford AT,

Delianides J, Baumann FG, Galloway AC, Colvin SB. 2004 Minimally invasive technology for mitral valve surgery via left thoracotomy: experience with forty cases. J Thorac Cardiovasc Surg. 127:1026-31

Segadal L, Matre K. Blood velocity distribution in the human ascending aorta Circul 1987; 76: 90-100

Shahcheraghi N, Dwyer HA, Cheer AY, Barakat AI, Rutaganira T.Unsteady and three-dimensional simulation of blood flow in the human aortic arch. J Biomech Eng 2002; 124: 378-387

Sharony R, Grossi EA, Saunders PC, Galloway AC, Applebaum R, Ribakove GH, Culliford AT.   Propensity case-matched analysis of off-pump coronary artery bypass grafting in patients with atheromatous aortic disease. J Thorac Cardiovasc Surg 2004;127:406–13.

Shiiya N, Yasuda K, Murashita T, Suto Y, Kanaoka T, Matsui Y, Sasaki S. Transapical aortic cannulation for hypothermic aortic operation through a left thoracotomy: an alternative to avoid retrograde arterial perfusion. J Thorac Cardiovasc Surg. 1997;113:1113-4

Steinberg D. An interpretive history of the cholesterol controversy: part I. J. Lipid Res. 2004. 45: 1583– 1593.

Svensson LG1, Blackstone EH, Rajeswaran J, Sabik JF 3rd, Lytle BW, Gonzalez-Stawinski G, Varvitsiotis P, Banbury MK, McCarthy PM, Pettersson GB, Cosgrove DM. Does the arterial cannulation site for circulatory arrest influence stroke risk? Ann Thorac Surg. 2004;78:1274-84

Tanemoto 1, Kuinose M, Kanaoka Y   (Complications of femoral artery cannulation in aortic arch related operations). Nihon Kyobu Geka Gakkai Zasshi. 1994; 42:306-10.

Ueda T, Shimizu H, Hashizume K, Koizumi K, Mori M, Shin H, Yozu R. Mortality and morbidity after total arch replacement using a branched arch graft with selective antegrade cerebral perfusion. Ann Thorac Surg 2003;76:1951–6.

Ura M, Sakata R, Nakayama Y, Goto T. Ultrasonographic demonstration of manipulation-related aortic injuries after cardiac surgery. J Am Coll Cardiol

2000;35:1303–10.

Vanierschot, M. & Van den Bulck, E. The influence of swirl on the reattachment length in an abrupt axisymmetric expansion. Int. J. Heat Fluid Flow 2008 ;9:75–82

Wada S, Yamamoto S, Honda J, Hiramoto A, Wada H, Hosoda Y. Transapical aortic cannulation for cardiopulmonary bypass in type A aortic dissection operations. J Thorac Cardiovasc Surg 2006; 132: 369–72

Wareing TH, Davila-Roman VG, Barzilai B, Murphy SF, Kouchoukos NT. Management of the severely atherosclerotic ascending aorta during cardiac operations. J Thorac Cardiovasc Surg. 1992; 103: 453-62

Weinstein GS. Left hemispheric strokes in coronary surgery: Implications for end-hole aortic cannulas. Ann Thorac Surg 2001; 71: 128-32

White JK, Jagannath A, Titus J, Yoneyama R, Madsen J, Agnihotri AK. Funnel-tipped aortic cannula for reduction of atheroemboli. Ann Thorac Surg. 2009;88:551-7.

Yamana K, Ito T, Maekawa A, Yoshizumi T, Sunada M, Hoshino S. Atherosclerotic arch aneurysm operations with perfusion toward the aortic valve. Ann Thorac Surg. 2010;89:435-9.

Yamanaka K, Miki S, Kusuhara K, Okita Y, Tahata T. The prevalence of atherosclerotic lesions in the aortic arch. Nihon Kyobu Geka Gakkai Zasshi. 1995;43:432-7

Yeawood TL. Chandran KB. Physiological pulsatile flow experiments in a model of the human aortic arch. J Biomech. 1984; 15: 683-704